Atmospheric Chemistry of 2-Amino-2-methyl-1-propanol: A Theoretical and Experimental Study of the OH-Initiated Degradation under Simulated Atmospheric Conditions

Wen Tan, Liang Zhu, Tomáš Mikoviny, Claus Nielsen, Yizhen Tang, Armin Wisthaler, Philipp Eichler, Markus Müller, Barbara D'anna, Naomi Farren, et al.

Atmospheric Chemistry of 2-Amino-2-methyl-1-propanol: A Theoretical and Experimental Study of the OH-Initiated Degradation under Simulated Atmospheric Conditions

Wen Tan,1 Liang Zhu,1 Tomáš Mikoviny,1 Claus J. Nielsen,1 Yizhen Tang,1 Armin Wisthaler,1 Philipp Eichler,2 Markus Müller,2 Barbara D´Anna,3 Naomi J. Farren,4 Jacqueline F. Hamilton,4 Jan B. C. Pettersson,5 Mattias Hallquist,5 Simen Antonsen6 and Yngve Stenstrøm6*

[1] Section for Environmental Sciences, Department of Chemistry, University of Oslo, P.O.Box. 1033 Blindern, NO-0315 Oslo, Norway.

[2] Institute of Ion Physics and Applied Physics, University of Innsbruck, 6020 Innsbruck, Austria

[3] Aix Marseille Univ, CNRS, LCE, UMR 7376, 13331, Marseille, France

[4] Wolfson Atmospheric Chemistry Laboratories, Department of Chemistry, University of York, York, YO10 5DD, United Kingdom.

[5] University of Gothenburg, Department of Chemistry and Molecular Biology, Atmospheric Science, 41296 Gothenburg, Sweden

[7] Faculty of Chemistry, Biotechnology and Food Science, Norwegian University of Life Sciences, P.O. Box 5003, N-1432 Ås, Norway.

ABSTRACT

The OH-initiated degradation of 2-amino-2-methyl-1-propanol [CH3C(NH2)(CH3)CH2OH, AMP] was investigated in a large atmospheric simulation chamber, employing time-resolved online high-resolution proton-transfer reaction-time-of-flight mass spectrometry (PTR-ToF-MS) and chemical analysis of aerosol online PTR-ToF-MS (CHARON-PTR-ToF-MS) instrumentation, and by theoretical calculations based on M06-2X/aug-cc-pVTZ quantum chemistry results and master equation modeling of the pivotal reaction steps. The quantum chemistry calculations reproduce the experimental rate coefficient of the AMP + OH reaction, aligning k(T) = 5.2 × 10−12 × exp (505/T) cm3 molecule−1 s −1 to the experimental value kexp,300K = 2.8 × 10−11 cm3 molecule−1 s −1 . The theoretical calculations predict that the AMP + OH reaction proceeds via hydrogen abstraction from the −CH3 groups (5−10%), −CH2− group, (>70%) and −NH2 group (5−20%), whereas hydrogen abstraction from the −OH group can be disregarded under atmospheric conditions. A detailed mechanism for atmospheric AMP degradation was obtained as part of the theoretical study. The photo-oxidation experiments show 2-amino-2-methylpropanal [CH3C(NH2)(CH3)CHO] as the major gas-phase product and propan-2-imine [(CH3)2C□NH], 2-iminopropanol [(CH3)(CH2OH)C□NH], acetamide [CH3C(O)NH2], formaldehyde (CH2O), and nitramine 2-methyl-2-(nitroamino)-1-propanol [AMPNO2, CH3C(CH3)(NHNO2)- CH2OH] as minor primary products; there is no experimental evidence of nitrosamine formation. The branching in the initial H abstraction by OH radicals was derived in analyses of the temporal gas-phase product profiles to be BCH3 /BCH2 /BNH2 = 6:70:24. Secondary photo-oxidation products and products resulting from particle and surface processing of the primary gas-phase products were also observed and quantified. All the photo-oxidation experiments were accompanied by extensive particle formation that was initiated by the reaction of AMP with nitric acid and that mainly

consisted of this salt. Minor amounts of the gas-phase photooxidation products, including AMPNO2, were detected in the particles by CHARON-PTR-ToF-MS and GC×GC-NCD. Volatility measurements of laboratory-generated AMP nitrate nanoparticles gave ΔvapH = 80 ± 16 kJ mol−1 and an estimated vapor pressure of (1.3 ± 0.3) × 10−5 Pa at 298 K. The atmospheric chemistry of AMP is evaluated and a validated chemistry model for implementation in dispersion models is presented

1 INTRODUCTION

2-Amino-2-methyl-1-propanol (AMP), $CH_3C(NH_2)(CH_3)CH_2OH$, is a common ingredient in many consumer products.[1] AMP is also one of the promising amines considered for usage in industrial scale post-combustion CO_2 capture technology due to its excellent absorption and desorption capacity, high loading capacity, and low replenishment cost.[2-4] A 40 wt% amine solution with piperazine and AMP in a 1:2 molar ratio has been suggested as the new benchmark solvent for CO_2 capture technology showing a cost reduction of 22% for coal-fired, and 15% for gas-fired power plants compared to a 30 wt% ethanolamine-based (MEA) system.[5]

Small amounts of solvent amines will invariably escape to the atmosphere during operation of a large-scale CO_2 capture facility employing amine technology. Once in the atmosphere, the amines undergo oxidative degradation resulting in the formation of imines, amides, and potential carcinogens such as nitrosamines and nitramines.[6] The Norwegian Institute for Public Health (NIPH) has recommended that *the total amount* of nitrosamines and nitramines in the atmosphere should be below 0.3 ng m^{-3} in air and below 40 ng dm^3 in drinking water for a risk level of 10^{-5}. [7] Such levels are extremely difficult to monitor, and it is consequently important to obtain

quantitative information on the degradation pathways for the relevant amines under atmospheric conditions, and to implement this information in reliable chemical models for dispersion calculations. Another important consideration is the contribution of amines to the formation of new particles.[8-9]

The rate coefficient for AMP reaction with OH radicals was reported to be $(2.8 \pm 0.5) \times 10^{-11}$ cm^3 $molecule^{-1}$ s^{-1} at 300 ± 2 K corresponding to an atmospheric lifetime around 10 h.[10] Environmental chamber experiments with AMP were initially carried out as so-called 'incremental reactivity' experiments to assess the ground-level atmospheric ozone impacts of consumer products.[11] In these experiments, AMP was added to a standard reactive organic gas surrogate - NO_X mixture simulating the chemical conditions of polluted urban atmospheres. AMP was characterized as very 'sticky' and a 'strong inhibitor of gas-phase reactions' causing a 'significant slowing of O_3 formation, NO oxidation and integrated OH radical levels'.[11] The experiments mentioned were severely hampered by wall loss and particle formation preventing amine quantification, and only a very simplified mechanism, having 80% H-abstraction from the $–NH_2$ group and including both nitrosamine and nitramine formation, was added to the SAPRC-07 mechanism.[12-13] A more detailed mechanism for AMP degradation was outlined from first principles by Bråthen et al.[14] as part of the Norwegian 'CO_2 and Amines Screening Study for Environmental Risks'.[15] Focusing on possible carcinogen formation, preliminary results from studies of AMP suggested a nitramine yield of (0.4 ± 0.2) % of reacted AMP per ppbV NO_2 present in the air.[16] A recent series of photo-oxidation experiments with AMP and surrogate hydrocarbon mixtures was carried out in the CSIRO 24.7 m^3 indoor smog chamber, and a more elaborate mechanism improving their prediction against AMP−VOC−NOx experiments was presented.[17]

Also these experiments encountered large amounts of AMP-derived secondary aerosol with a reported mass yield of 1.06 ± 0.20.

We have recently presented results from theoretical calculations and experimental photo-oxidation studies of piperazine [18] – the other component of the suggested new benchmark solvent for CO_2 capture technology – and previously reported results from theoretical and experimental photo-oxidation studies of the AMP related, simpler compound *tert*-butylamine, $(CH_3)_3C(NH_2)$.[19] The present communication summarizes our results from detailed theoretical calculations of AMP degradation under atmospheric conditions, and from photo-oxidation experiments carried out under simulated atmospheric conditions in the 200 m^3 European Photoreactor (EUPHORE) in Spain.

2 METHODS

2.1 Experimental Methods and Chemicals

A series of experiments was carried out in chamber B of the EUPHORE facility in Valencia, Spain. The facility and analytical methods have previously been reported in detail;[20] special on-line instrumentation employed in the present experiments include a high-resolution PTR-TOF 8000 instrument ($m/\Delta m$ > 3000) from Ionicon Analytik GmbH, a prototype CHARON inlet [21,22] interfaced to a second PTR-TOF 8000 ($m/\Delta m$ > 3000), and a C-ToF-AMS from Aerodyne Research Inc.[23] Additional information specific to the present work is found in the Supporting Information.

AMP (Sigma-Aldrich, ReagentPlus®, ≥99%), Ammonium Nitrate (Sigma-Aldrich) and 2-methylpropane-1,2-diol (Apollo Scientific Ltd, 99.97%) were used as received. 2-Propyl nitrite (isopropyl nitrite, IPN) was synthesized from isopropanol, hydrochloric acid and sodium nitrite, and purified by repeated washing with ice water. The AMP nitrate salt was prepared by adding an

excess of diluted nitric acid (HNO_3) to diluted AMP followed by rotary evaporation to dryness at 80 °C. 2-Methyl-2-(nitroamino)-1-propanol ($AMPNO_2$) was prepared as described by Antonsen et al.,[24] see the Supporting Information for details.

2.2 Computational Methods

Optimized geometries of stationary points on the potential energy surface of the OH reaction with AMP were obtained with the M06-2X hybrid meta exchange-correlation density functional [25] employing the aug-cc-pVTZ basis sets [26-27] and tight optimization criteria and ultrafine integration grids. Pre and post reaction complexes were located by following the reaction path (IRC) from the saddle points. Electronic energies of selected stationary points were improved by explicitly correlated coupled cluster calculations with scaled triples contributions, denoted CCSD(T*)-F12a.[28] Reaction enthalpies and proton affinities were calculated using the G4 model chemistry.[29] Dipole moments and isotropic polarizabilities serving as input to the prediction of ion-molecule reaction rate coefficients [30] were obtained in B3LYP [31-34] and M06-2X calculations. The DFT and G4 calculations were done with Gaussian 09 [35] and Gaussian 16,[36] CCSD(T*)-F12a calculations were performed employing Molpro 2012.1.[37]

Master equation calculations were carried out using MESMER 3.0 [38] to simulate the reactions at atmospheric conditions. The required input parameters for molecules, intermediate species and products were obtained from the ab initio calculations.

3 RESULTS & DISCUSSION

We first report results from a theoretical study of the OH-initiated photo-oxidation of AMP under atmospheric conditions facilitating presentation and interpretation of the experimental data. We then show results from gas phase photo-oxidation experiments, before addressing the results for the particle phase, and finally attending to modelling the chamber experiments.

3.1 Computational results

AMP exists in several conformations; the lowest energy conformer has the OH and NH_2 groups in a *gauche* configuration with an intramolecular H-bonding from the OH-group to the NH_2-group. There are two additional AMP conformers within 10 kJ mol^{-1}, in which the NH_2-group is the proton donor, but these conformers will only be populated a few per cent under atmospheric conditions, and they will not be considered here.

There are four avenues in the AMP + OH reaction; in decreasing order of the reaction enthalpy (in units of kJ mol^{-1} at 298 K) they are:

ΔH^{Θ} = -105 $CH_3C(NH_2)(CH_3)CH_2OH + OH \rightarrow CH_3C(NH_2)(CH_3)\dot{C}HOH + H_2O$ (1a)

ΔH^{Θ} = -78 $\rightarrow CH_3C(\dot{N}H)(CH_3)CH_2OH + H_2O$ (1b)

ΔH^{Θ} = -71 $\rightarrow \dot{C}H_2C(NH_2)(CH_3)CH_2OH + H_2O$ (1c)

ΔH^{Θ} = -56 $\rightarrow CH_3C(NH_2)(CH_3)CH_2\dot{O} + H_2O$ (1d)

AMP has 11 non-equivalent H-atoms, and a thorough theoretical description of the AMP + OH reaction kinetics is consequently far from trivial. Figure 1 illustrates the relative energies of stationary points on the entrance side of the potential energy surfaces (PESes) of the four routes – detailed figures, electronic energies, Cartesian coordinates and vibration-rotation data for all stationary points on the PESes of reaction 1 are collected in Figures S5-S7 and Table S2. The reaction is characterized by pre- and postreaction complexes and several saddle points to reaction below the entrance energy of the reactants. The barrier to abstraction from the –OH group is calculated to be around 10 kJ mol^{-1}, and this route will consequently be of little importance under atmospheric conditions.

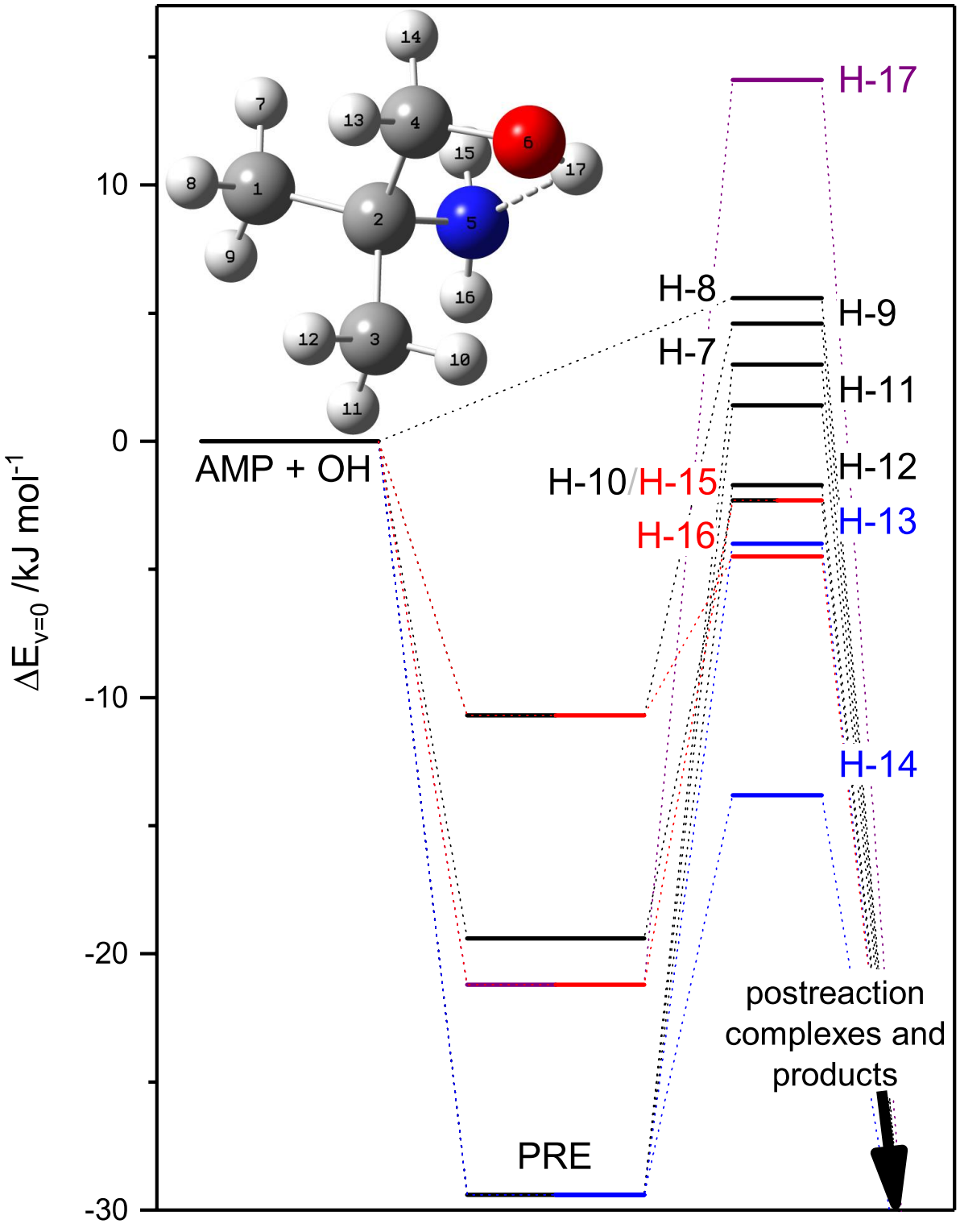

Figure 1. Relative energies of stationary points on the potential energy surface of the AMP + OH reaction. Results from M06-2X/aug-cc-pVTZ calculations. The CH_3-abstraction routes are

outlined in black color, the CH_2-abstraction routes in blue, the NH_2-abstraction routes in red, and the OH-abstraction route in purple color. For clarity, the stationary points of postreaction complexes and products are not included in the figure.

The kinetics of reaction 1 was simulated in a master equation model based on the PES illustrated in part in Figure 1 (all vibrational modes were treated as harmonic oscillators). Spin-orbit coupling in the OH radical (139.7 cm^{-1}) [39] was included in the model by lowering the energy of the OH radical with half of the splitting and including the $^2\Pi_{3/2}$ and $^2\Pi_{1/2}$ spin-orbit states in the electronic partition function; it was assumed that spin-orbit coupling could be neglected in pre-reaction adducts and in the saddle points. The formation of pre-reaction complexes and dissociation of post-reaction complexes were treated as reversible reactions with rate coefficients approximated by typical values of $k_{association} = 4 \times 10^{-10} \times (T/298\ K)^{-1/6}$ cm^3 $molecule^{-1}$ s^{-1} from long-range transition state theory (LRTST).[40] Tunneling was included using a one dimensional asymmetric Eckart potential.[41] The calculations predict a rate coefficient $k_{AMP+OH} = 3.6 \times 10^{-11}$ cm^3 $molecule^{-1}$ s^{-1} at 298 K, which, by utter fortuity, is close to the experimental value of $(2.8 \pm 0.5) \times 10^{-11}$ cm^3 $molecule^{-1}$ s^{-1} at 300 K.[10] The branching between H-abstraction from the $–CH_3$ groups, and the $–CH_2–$ and $–NH_2$ groups is predicted to be 5 : 90 : 5 at 298 K; H-abstraction from the –OH group will contribute with less than 0.1 % to the total reactivity and clearly be of little importance under atmospheric conditions. The LRTST value for $k_{association}$ is an upper case value and reducing $k_{association}$ by a factor of 4 in the model changes the branching to 7 : 86 : 7 and the predicted rate coefficient to 2.7×10^{-11} cm^3 $molecule^{-1}$ s^{-1} at 298 K. The calculated overall rate coefficient has virtually no pressure dependence in the 1 – 1000 mbar region and shows a negative temperature dependency. The theoretical results can be reasonably well described by the Arrhenius equation,

and aligning the theoretical results to the experimental rate coefficient at 300 K results in $k(T) = 5.2 \times 10^{-12} \times \exp(505/T)$.

The OH reaction with the related compound, *tert*-butylamine (tBA), was previously examined in both M062X and MP2 calculations.[19] In addition, improved single point energies were obtained in CCSD(T*)-F12a calculations. In general, the results for the tBA + OH reaction obtained in M062X, CCSD(T*)-F12a //M062X and CCSD(T*)-F12a//MP2 agreed within 2 kJ mol^{-1} when the aug-cc-pVTZ basis set was employed. The exception being the energy of the saddle point to N-H abstraction, which was calculated 4 kJ mol^{-1} lower at the CCSD(T*)-F12a//MP2 level.

The sensitivity of the calculated rate coefficient and the branching to variations in the saddle point energies was examined by varying all barrier heights by ± 2 kJ mol^{-1}. The results show that changing all barriers ± 2 kJ mol^{-1} results in a $^{-}$,$_{+}$ 45% change in the calculated rate coefficient at 298 K. At the same time the branching changed from 5.5 : 89.5 : 5.0 to respectively 7.6 : 85.0 : 7.4 and 4.6 : 91.2 : 4.2. Changing only the barriers to H-abstraction from the –NH_2 group by ± 4 kJ mol^{-1}, alters the rate coefficient by respectively -4 and +16%, and the branching correspondingly to 5.6 : 93.4 : 1.0 and 4.7 : 77.3 : 18.0. The theoretical calculations consequently place conservative upper limits of ~10% to abstraction from the –CH_3 groups and ~20% to abstraction from the –NH_2 group. The present result for the branching in the AMP + OH reaction therefore differs radically from that currently employed in air quality models, which both adopt 80% abstraction from the –NH_2 group.[11, 17]

A detailed account of our theoretical study of the atmospheric fate of the $CH_3C(\dot{N}H)(CH_3)CH_2OH$, $CH_3C(NH_2)(CH_3)\dot{C}HOH$, $\dot{C}H_2C(NH_2)(CH_3)CH_2OH$ and $CH_3C(NH_2)(CH_3)CH_2\dot{O}$ radicals is found in the Supporting Information, which includes figures of pivotal reaction steps (Figures S8-S16) and associated tables containing electronic energies,

Cartesian coordinates and vibration-rotation data (Tables S3 – S11). The theoretically predicted atmospheric degradation routes are outlined in Scheme 1, from which it can be seen that there are characteristic primary products to each route, and that $CH_3C(NH_2)(CH_3)CHO$ is predicted to be the major product in AMP photo-oxidation under atmospheric conditions.

Rate coefficients for the OH reactions with $(CH_3)_3CCH_2OH$ ($k_{OH} = 5.2 \times 10^{-12}$ cm^3 molecule^{-1} s^{-1} at 298 K) [42] and $(CH_3)_3CCHO$ ($k_{OH} = 2.7 \times 10^{-11}$ cm^3 molecule^{-1} s^{-1} at 298 K) [43] show the –CHO group being around 5 times more reactive than the $–CH_2OH$ group. This, in turn, implies that $CH_3C(NH_2)(CH_3)CHO$ should react at least twice as fast with OH radicals as AMP does, and that aldehydic H-abstraction will be the dominant route:

$\Delta H^{\Theta} = -125$ $\quad CH_3C(NH_2)(CH_3)CHO + OH \rightarrow (NH_2)(CH_3)_2C\dot{C}O + H_2O$ (2)

The quantum chemistry calculations (Figure S17, Table S12) show the barrier to dissociation of the carbonyl radical being only ~14 kJ mol^{-1}, which places the thermal dissociation rate at 6×10^8 s^{-1} at 298 K:

$\Delta H^{\Theta} = +18$ $\quad (NH_2)(CH_3)_2C\dot{C}O \xrightarrow{\Delta,} (NH_2)(CH_3)_2\dot{C} + CO$ (3)

A simplified master equation calculation, assuming equipartitioning of the enthalpy of reaction 2, shows the lifetime of the vibrationally excited $(NH_2)(CH_3)_2C\dot{C}O^{\ddagger}$ radical to be less than 10^{-10} s under atmospheric conditions. The rate coefficient for the competing reaction with O_2, $(NH_2)(CH_3)_2C\dot{C}O + O_2 \rightarrow (NH_2)(CH_3)_2CC(O)O\dot{O}$, is around 5×10^{-12} cm^3 molecule^{-1} s^{-1} (k_{∞,CH_3CO+O_2} [44]) making it several orders of magnitude slower than the dissociation. The formation of peroxyacyl radicals and the peroxyacylnitrate can consequently be neglected.

Scheme 1. Major reaction routes for the OH initiated photo-oxidation of AMP under atmospheric conditions. Thermally stable products are typeset in bold blue font. Radical sites are indicated in red font.

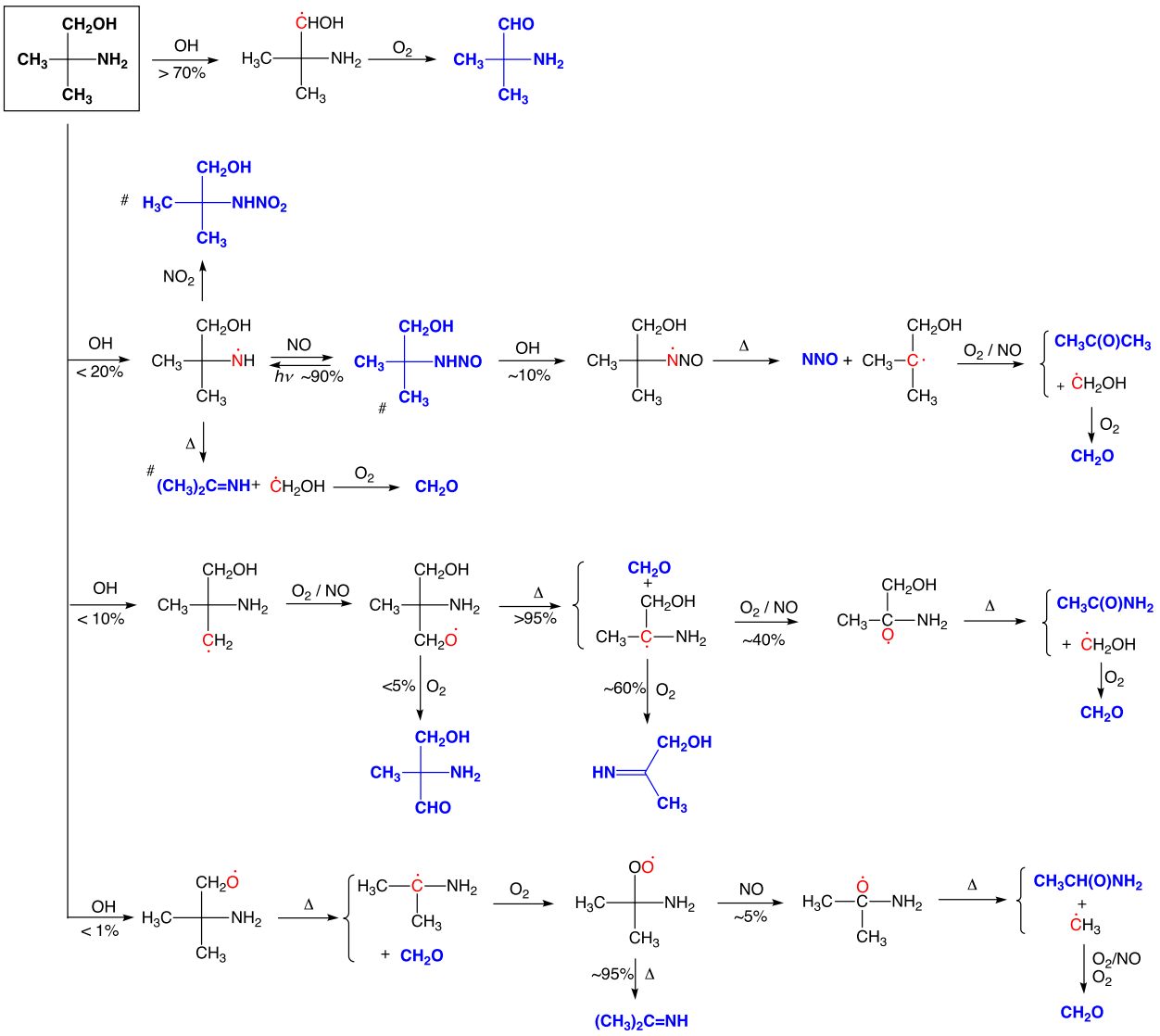

The branching depends upon the NO and NO_2 mixing ratios.

Focusing on nitrosamine and nitramine formation following reaction 1b, the theoretical calculations (CCSD(T*)-F12a/aug-cc-pVTZ//M06-2X/aug-cc-pVTZ) forecast the aminyl radical, $CH_3C(\dot{N}H)(CH_3)(CH_2OH)$, with a relatively low barrier to dissociation of only 83.7 kJ mol^{-1}:

ΔH^{Θ} = +68 $\quad CH_3C(\dot{N}H)(CH_3)(CH_2OH) \xrightarrow{\Delta} (CH_3)_2C{=}NH + \dot{C}H_2OH$ (4)

RRKM calculations predict reaction 2 with a thermal rate coefficient of 4.3×10^{-2} s^{-1} at 298 K, which is comparable to the rates of the competing reactions with NO and NO_2 under atmospheric conditions.[45-46] The theoretical calculations also show that O_2, due to the lack of hydrogen atoms in α-position, is *not* a sink for the aminyl radical under atmospheric conditions, and that AMPNO (a *primary* nitrosamine) is thermally stable in the gas phase; the potential energy surface for dissociation reactions via the nitrosamine-hydroxydiazene isomerization[47-48] is complex with 2 nitrosamine and 4 low energy hydroxydiazene conformers, and barriers effectively blocking any significant dissociation under atmospheric conditions:

ΔH^{Θ} = -9 $\quad (CH_3)_2(CH_2OH)CNHNO \rightleftarrows (CH_3)_2(CH_2OH)CN{=}NOH$ (5)

ΔH^{Θ} = +52 $\quad (CH_3)_2(CH_2OH)CN{=}NOH \xrightarrow{\Delta} (CH_3)_2C{=}N{=}N + CH_2O + H_2O$ (6)

Finally, the theoretical study finds the OH radical to react extremely fast with both the nitrosamine and the hydroxydiazene, $k_{OH} > 1 \times 10^{-10}$ cm^3 $molecule^{-1}$ s^{-1} at 298 K, resulting in the formation of nitrous oxide.

3.2 Experimental results

Seven photo-oxidation experiments were carried out under different conditions; p, T, RH, O_3, NO, NO_2 mixing ratios, j_{NO2}, and particle mass loadings are detailed in Table S13 and Figures S18–S24. The experiments are characterized by a low relative humidity between 1.5 and 2% (dewpoint temperature around -30 °C). All experiments were accompanied by extensive particle formation that was initiated by the reaction of AMP with nitric acid, and that mainly consisted of

this salt; in some experiments up to 50% of AMP was transferred from the gas phase to the particle phase.

3.2.1 Gas-phase photo-oxidation products

The PTR-ToF-MS was operated with alternating the drift tube electric field between *E/N* = 65 and 105 Td to recognize ion fragmentation facilitating the interpretation. At *E/N*= 65 Td AMP is detected at *m/z* 90.092 (87.7%, $C_4H_{12}NO^+$), 73.065 (2.3%, $C_4H_9O^+$, NH_3 ejection), 72.081 (1.6%, $C_4H_{10}N^+$, H_2O ejection) and 18.035 (8.4%, NH_4^+); at *E/N*= 105 the fragmentation is 55.5% *m/z* 90.092, 6.0% *m/z* 73.065, 5.5% *m/z* 72.081 and 33.0% *m/z* 18.035 (the relative intensities of low m/z peaks are not corrected for instrument mass discrimination). Protonated $AMPNO_2$ undergoes more extensive fragmentation; calibration experiments show the major ion signal at *m/z* 73.065 (62%, $C_4H_9O^+$, ejection of NH_2NO_2), whereas the protonated molecule ($C_4H_{11}N_2O_3^+$) at *m/z* 135.076 only accounts for 38% of the total ion intensity at *E/N* = 65 Td (at *E/N*= 105 Td the *m/z* 135.076 signal was below detection level in the chamber measurements). AMP is a 'sticky' molecule. However, the time-profiles of AMP, obtained by the PTR-ToF-MS and a High-Temperature PTR-QMS instrument, compare well showing an appropriate time-response for product studies (Figure S25).

Figure 2 exemplifies the results from an experiment carried out under initial low-NOx conditions. In this particular experiment the initial NOx-level was around 15 ppbV, which slowly increased throughout the experiment as IPN was injected into the chamber to maintain a reasonably high OH level in the experiments ($CH_3CH(ONO)CH_3 \xrightarrow{h\nu} CH_3CH(\dot{O})CH_3 + NO$; $CH_3CH(\dot{O})CH_3 + O_2 \rightarrow CH_3C(O)CH_3 + HO_2$; $HO_2 + NO \rightarrow OH + NO_2$). Around 10 minutes after opening the canopy exposing the chamber to solar radiation, IPN was injected with a flow of 0.3 µL min^{-1} in a stream of N_2 into the chamber for 10 min (~0.4 ppbV min^{-1}). The flow was then reduced to 0.1 µl min^{-1}

until the chamber canopy was closed, at which time a total of 16 µL IPN had been added to the chamber. The observed ion signals, relevant to AMP photo-oxidation, are presented in Table 1 together with our interpretation. Only ion signals having an intensity >2% of the decrease in the AMP signal *m/z* 90.092 during the time the chamber canopy was open are included in the table.

It is instantly recognized from Figure 2 that three of the ion signals, growing in during the AMP photo-oxidation, have very distinct temporal profiles: *m/z* 73.065, 135.074 and 103.049. It is obvious that there have to be supplement contributors to *m/z* 73.065 in addition to AMP and $AMPNO_2$, see above. The two other signals, of which *m/z* 135.074 is indicative of $AMPNO_2$, appear slightly delayed relative to the other ion signals, and both are growing in intensity throughout every experiment – even after closing the chamber canopy to solar radiation – indicating at least some relationship to heterogeneous chemistry reactions in the chamber.

The NO_3 radical may likely contribute to the chamber reactions. Whereas the NO_3 radical photolyzes quickly under sunlight conditions ($NO_3 + h\nu \rightarrow NO + O_2$) never reaching significant levels, the NO_3 radical concentration will build up under dark conditions upon closing the chamber canopy. The NO_3 radical concentration, calculated from the observed NO, NO_2 and O_3 concentrations (see Figures S18 – S24),[49] is ~4×10^7 cm^{-3} just after closing the chamber canopy increasing to ~7×10^7 cm^{-3} within 10 minutes and then decreasing to ~6×10^7 cm^{-3} the next 30 min. There is no experimental value for k_{NO_3+AMP}, but the empirical correlation between OH and NO_3 rate coefficients for reaction with amines implies a moderate rate coefficient, $k_{NO_3+AMP} \approx 3.7 \times 10^{-14}$ cm^3 $molecule^{-1}$ s^{-1} at 298 K.[6] It can therefore be concluded that NO_3 radical reactions will not be important in the illustrated experiment.

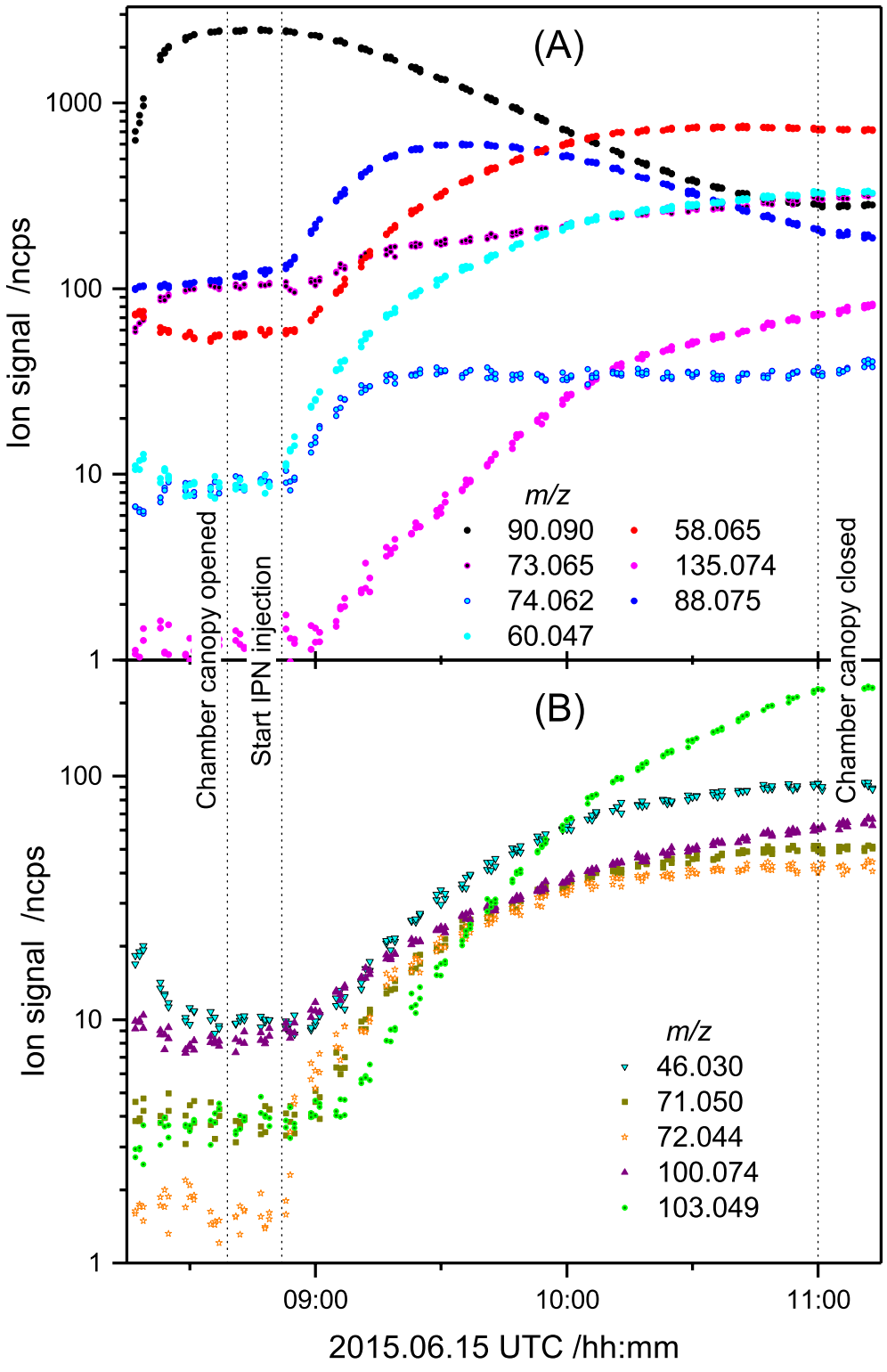

Figure 2. Major ion signals observed at E/N = 65 Td during the AMP photo-oxidation experiment on 2015.06.15. (A) Ion signal of AMP and primary products in the AMP + OH reaction. For clarity,

the AMP fragment ion signal at *m/z* 72.081 is omitted. (B) Ion signals of secondary products. The *m/z* 74.062 raw signal shown is not corrected for the isotope contribution of *m/z* 73.065.

H-abstraction from the –CH₂– group in AMP is predicted in the theoretical calculations to account for more than 70% of the AMP + OH reaction. In accordance, one of the largest ion signals observed in all experiments, *m/z* 88.076 ($C_4H_{10}NO^+$), is attributed to 2-amino-2-methylpropanal, $CH_3C(NH_2)(CH_3)CHO$.

The distinct transient profile of *m/z* 88.076 is typical for a reactive product. Rate coefficients for the OH reactions with $(CH_3)_3CCH_2OH$ (k_{OH} = 5.2 × 10^{-12} cm^3 $molecule^{-1}$ s^{-1} at 298 K) [42] and $(CH_3)_3CCHO$ (k_{OH} = 2.7 × 10^{-11} cm^3 $molecule^{-1}$ s^{-1} at 298 K) [43] show the –CHO group being around 5 times more reactive than the $–CH_2OH$ group. This, in turn, implies that $CH_3C(NH_2)(CH_3)CHO$ should react at least twice as fast with OH radicals as AMP does, and that aldehydic H-abstraction will be the dominant route. The *m/z* 88.076 profile gives a somewhat deceptive visual impression of the actual –CH₂– abstraction yield – the maximum signal intensity, occurring after around 1 h of reaction, is actually less than half of what it would have been, had the compound not reacted with OH.

The theoretical study shows that aldehydic H-abstraction from $CH_3C(NH_2)(CH_3)CHO$ leads to the tertiary $(CH_3)_2(NH_2)\dot{C}$ radical and not to formation of an intermediate peroxyacylnitrate, $(CH_3)_2(NH_2)CC(O)OONO_2$. This is corroborated by peroxy radical titration at the end of each photo-oxidation experiment, in which the addition of excess NO produces no correlated changes in the ion signals.

The $(CH_3)_2(NH_2)\dot{C}$ radical is also pivotal in the reactions following H-abstraction from the OH group in AMP, Scheme 1. Two products arise: ~95% $(CH_3)_2C{=}NH$ and ~5% $CH_3C(O)NH_2$. In

agreement, the second-largest product signal observed, *m/z* 58.065 ($C_3H_8N^+$), is attributed to $(CH_3)_2C{=}NH$. The other product, acetamide, is expected to be identified and quantified at *m/z* 60.044 ($C_2H_6NO^+$) despite strong ion signals, caused by the use of IPN as OH precursor – *m/z* 59.049 ($C_3H_7O^+$, 100%) and isotopes 60.053 (3.3%) and 61.056 (0.1%) – complicate the spectral interpretation. The acetone isotopes were taken into consideration when estimating the concentration of acetamide.

Whereas acetamide reacts slowly with OH radicals (k_{OH} = 7.5 ×10^{-13} cm^3 $molecule^{-1}$ s^{-1} at 298 K), [50] propane-2-imine is foreseen to undergo further reaction during the experiments. There exist no experimental data for imine gas phase reactions with OH radicals in the literature, but two theoretical studies of the atmospheric chemistry of the simplest imine, $CH_2{=}NH$,[51-52] predict that its rate coefficient for reaction with OH is ~3 × 10^{-12} cm^3 $molecule^{-1}$ s^{-1}, which is equally fast as AMP. Further, the reaction was projected to be completely dominated by hydrogen abstraction with around 50% N-H abstraction. Methyl groups are in general not very reactive towards OH radicals, and the main route in the $(CH_3)_2C{=}NH$ + OH reaction is therefore expected to be N-H abstraction. Again, following the results from the theoretical study on the atmospheric chemistry of $CH_2{=}NH$,[51] the $(CH_3)_2C{=}\dot{N}$ radical may either eject $\dot{C}H_3$, resulting in CH_3CN, or react with NO or NO_2, resulting in $(CH_3)_2C{=}NNO$ and $(CH_3)_2C{=}NNO_2$, respectively. Acetonitrile is a frequent background contaminant in many laboratories running HPLC instrumentation. However, *m/z* 42.034 was detected within the 2% cutoff limit in 3 of 6 experiments with temporal profiles consistent with CH_3CN being a product in the AMP photo-oxidation. The two other potential products, $(CH_3)_2C{=}NNO$ and $(CH_3)_2C{=}NNO_2$, are expected to show up in PTR-MS at *m/z* 87.056 (or 56.050, HNO-ejection) and 103.049 (or 56.050, HOHO/HNO_2-ejection), respectively. Of these, only the *m/z* 103.049 signal was detected within the 2% cutoff limit in 5 of 6 experiments;

in all instances the temporal profiles appear slightly delayed relative to the other ion signals and growing in intensity throughout the experiments.

H-abstraction from the $–NH_2$ group in $CH_3C(NH_2)(CH_3)CHO$ is, by analogy to the $CH_3C(NH_2)(CH_3)CH_2OH$ reactions (see below), expected to result in $(CH_3)(CHO)C=NH$, $(CH_3)_2(CHO)CNHNO$, and $(CH_3)_2(CHO)CNHNO_2$. 2-Iminopropanal ($CHO(CH_3)C=NH$), is recognized by the small *m/z* 72.044 signal ($C_3H_6NO^+$) showing a growth slightly delayed relative to the *m/z* 88.076 signal of $CH_3C(NH_2)(CH_3)CHO$. Assuming that protonated $(CH_3)_2(CHO)CNHNO_2$ undergoes extensive fragmentation similar to that of $AMPNO_2$, the major ion signal from protonated $(CH_3)_2(CHO)CNHNO_2$ is expected at the observed *m/z* 71.049. Although the signal of the protonated molecule (*m/z* 133.061) is not observed we tentatively attribute *m/z* 71.049 to the secondary nitramine product $(CH_3)_2(CHO)CNHNO_2$. We find no evidence of the nitrosamine, $(CH_3)_2(CHO)CNHNO$, in any of the experiments.

H-abstraction from the –NH₂ group in AMP is projected by the theoretical calculations to account for less than 20% of the AMP + OH reaction; the anticipated products are: CH_2O, $(CH_3)_2C=NH$, $AMPNO_2$ and AMPNO. Formaldehyde, which is a common chamber artefact, was detected at *m/z* 31.018 (CH_3O^+) by PTR operated with *E/N* = 105 Td. The temporal profiles of formaldehyde clearly show the compound to be a primary product in all experiments. However, formaldehyde is not a product unique to the N-H abstraction route. The same is true for propan-2-imine, $(CH_3)_2C=NH$, that is also a secondary photo-oxidation product following H-abstraction from the $–CH_2–$ group, see above.

The PTR-MS signals of $AMPNO_2$, *m/z* 73.065 ($C_4H_9O^+$) and 135.076 ($C_4H_{11}N_2O_3^+$), were detected in all experiments. As mentioned, the *m/z* 135.076 ion signal grows in intensity throughout every experiment, which is not consistent with its origin being a molecular species only

produced in the gas phase. The *m/z* 73.065 ion signal, which has contributions from AMP as well as other species (see below), does therefore not constitute an unambiguous identification of $AMPNO_2$ resulting from gas phase chemistry. We note that Li et al.[17] identified $AMPNO_2$ in their AMP photo-oxidation experiments by SIFT-QMS through *m/z* 164, which is the ion-molecule product of $AMPNO_2$ with reagent ion NO^+.

Concerning AMPNO, it is known from aqueous phase chemistry that nitrosamines from primary amines are very unstable,[53] and that they quickly react (acid catalyzed) to the corresponding alcohols: ($R\text{-}NHNO_{(aq)} \rightarrow,\leftarrow R\text{-}N{=}NOH_{(aq)}$; $R\text{-}N{=}NOH_{(aq)} + H^+_{(aq)} \rightarrow,\leftarrow R\text{-}N{=}NOH^+_{2\,(aq)} \rightarrow R^+_{(aq)} + N_2 + H_2O \rightarrow ROH_{(aq)} + N_2 + H^+_{(aq)}$). The theoretical calculations, however, predict AMPNO to be thermally stable in the gas phase and indicates a lifetime of around 500 s in the chamber experiments, see the Supporting Information. The theoretical study also indicates that around 50% of the AMPNO formed will react with OH radicals under the conditions in the chamber experiments resulting in $CH_3C(O)CH_3$, CH_2O and N_2O.

It was not possible to verify the formation and the existence of AMPNO in the gas phase explicitly by PTR-MS in any of the present experiments. Both acetone and formaldehyde are common chamber artefacts, and both also have other sources in the AMP photo-oxidation. Nitrous oxide cannot be detected by PTR and the FTIR employed was not sensitive enough to reveal single digit ppbV amounts of N_2O being formed in the photo-oxidation experiments.

One possible explanation to the failure of PTR-MS detecting the protonated molecule of AMPNO is that protonated AMPNO fragments readily; quantum chemistry calculations show that HNNOH fragmentation reaction has no electronic barrier in addition to $\Delta_{fragment}E_0$:

$\Delta H^{\Theta} = -182$ $\quad (CH_3)_2C(NHNO)CH_2OH + H_3O^+ \rightarrow [(CH_3)_2C(NHNO)CH_2OH]H^+ + H_2O$ $\quad (7)$

ΔH^{Θ} = $[(CH_3)_2C(NHNO)CH_2OH]H^+ \xrightarrow{\Delta} (CH_3)_2CCH_2OH^+ + HNNOH$ (8a)
+154

ΔH^{Θ} = $\xrightarrow{\Delta} (CH_3)_2\dot{C}CH_2OH + HNNOH^+$ (8b)
+509

Further, the resulting cation signal ($(CH_3)_2CCH_2OH^+$, *m/z* 73.065) has also contributions from both protonated AMP and $AMPNO_2$.

A second explanation is linked to nitrosamine hydrolysis in the chamber and/or in the PTR-MS detection system, in the present case resulting in 2-methylpropane-1,2-diol. Laboratory experiments, employing a validated $CH_3C(OH)(CH_3)CH_2OH$ sample show two ion signals *m/z* 91.076 (~30%) and 73.065 (~70%, H_2O ejection) at *E/N* = 65 Td. The AMP isotope signals (*m/z* 91.089, 91.095, 91.098) coalesce at *m/z* 91.092, and the only ion signal observed in the vicinity of *m/z* 91.076 is an extremely weak peak at *m/z* 91.051 that shows a relatively flat temporal profile. The *m/z* 73.065 signal also has contributions from both AMP and $AMPNO_2$ in our experiments.

A third explanation is simply that the nitrosamine level in the experiments was below the PTR-MS detection limit (~50 pptV). In any case, the *m/z* 135.076 ion signal is the only experimental indication of H-abstraction from the $–NH_2$ group in the gas phase.

H-abstraction from the –CH₃ groups in AMP is predicted to account for less than 10 % of the AMP + OH reaction. Four products are anticipated to appear in this route: CH_2O, $CH_3C(O)NH_2$, $HN=C(CH_3)CH_2OH$ and $(CH_3)(CHO)(CH_2OH)CNH_2$; the latter two are unique to this path. The imine, $HN=C(CH_3)CH_2OH$, is recognized by the ion signal *m/z* 74.060 ($C_3H_8NO^+$) that is showing a temporal profile indicating secondary reactions during the experiments. The compound is expected to be more reactive than $(CH_3)_2C=NH$ – the increased reactivity being associated with the $–CH_2–$ group. The reaction with OH radicals will therefore primarily lead to $(CH_3)(CHO)C=NH$, which we tentatively ascribe to the PTR-MS signal *m/z* 72.044 ($C_3H_6NO^+$).

Finally, $HOCH_2C(NH_2)(CH_3)CHO$, which is predicted to account for less than 5% of the products following H-abstraction from the $–CH_3$ groups, was not discovered among the products.

3.2.2 Heterogeneous chemistry products

Amines are known to form imines in condensation reactions with carbonyl compounds in solution,[54] and on surfaces.[55] Primary amines attached to a tertiary alkyl group give 'stable' imines with primary aldehydes as steric hindrance makes aldol condensations difficult.[54] The present experiments show three small ion signals *m/*z 100.075 ($C_5H_{10}NO^+$), 102.089 ($C_5H_{12}NO^+$) and 116.070 ($C_5H_{10}NO_2^+$) all corresponding to molecules having one more carbon atom than AMP itself. The *m/*z 100.075 and 116.070 signals are delayed relative to gas phase product signals and grow in intensity throughout the experiments, whereas *m/*z 102.089 appears early and decreases again later in the experiments. The *m/*z 102.089 is recognized from laboratory experiments as the AMP condensation product with formaldehyde:[56]

$$(CH_3)_2(CH_2OH)CNH_{2(sur)} + CH_2O_{(sur)} \leftarrow,\rightarrow (CH_3)_2(CH_2OH)CN{=}CH_{2(sur)} + H_2O_{(sur)} \quad (9)$$

Similarly, the *m/*z 100.075 is attributed to condensation between the major, primary product $(CH_3)_2(CHO)CNH_2$ and formaldehyde:

$$(CH_3)_2(CHO)CNH_{2(sur)} + CH_2O_{(sur)} \leftarrow,\rightarrow (CH_3)_2(CHO)C\text{-}N{=}CH_{2(sur)} + H_2O_{(sur)} \quad (10)$$

The *m/*z 116.070 ($C_5H_{10}NO_2^+$) is tentatively ascribed to the formic acid ester of AMP

$$(CH_3)_2(NH_2)CCH_2OH_{(sur)} + HC(O)OH_{(sur)} \leftarrow,\rightarrow (CH_3)_2(NH_2)CCH_2OC(O)H_{(sur)} + H_2O_{(sur)} \quad (11)$$

Amines also undergo addition reactions with organic acids. Formic acid is omnipresent is chamber experiments, and its reaction with AMP results in the formation of an oxirane (2,2-dimethyloxirane) and formamide, see Scheme S5. The oxirane can also be formed in an *intra* molecular AMP reaction:

$$(CH_3)_2(NH_2)CCH_2OH_{(sur)} + HC(O)OH_{(sur)} \leftarrow,\rightarrow CH_2(O)C(CH_3)_{2(sur)} + CHONH_{2(sur)} \quad (12)$$

$$(CH_3)_2(NH_2)CCH_2OH_{(sur)} \leftarrow,\rightarrow CH_2(O)C(CH_3)_{2(sur)} + NH_{3(sur)} \quad (13)$$

In PTR-MS the oxirane (C_4H_8O) will show up as the protonated molecular ion at *m/z* 73.065, which also has contributions from both AMP and $AMPNO_2$. The presence of formamide, to which there are no obvious chemical routes in AMP gas phase photo-oxidation, is evidenced by m/z 46.029 that was observed in 5 of the 6 experiments with temporal profiles resembling those of secondary products, Figure 2.

As mentioned, the two ion signals *m/z* 103.049 ($C_3H_7N_2O_2^+$) and 135.074 ($C_4H_{11}N_2O_3^+$) show very similar temporal profiles indicating contributions from heterogeneous chemistry reactions. The former is attributed to $(CH_3)_2C{=}NNO_2$, the latter to $AMPNO_2$. In addition to the abovementioned gas phase routes leading to these two compounds, simple surface reactions (mechanisms illustrated in Scheme S5) involving HNO_3 are likely to take place:

$$(CH_3)_2C{=}NH_{(sur)} + HNO_{3(sur)} \leftarrow,\rightarrow (CH_3)_2C{=}NNO_{2(sur)} + H_2O_{(sur)} \quad (14)$$

$$(CH_3)_2(NH_2)CCH_2OH_{(sur)} + HNO_{3(sur)} \leftarrow,\rightarrow (CH_3)_2(NH_2)CCH_2ONO_{2(sur)} + H_2O_{(sur)} \quad (15a)$$

$$\leftarrow,\rightarrow (CH_3)_2(CH_2OH)CNHNO_{2(sur)} + H_2O_{(sur)} \quad (15b)$$

Alkylnitrates fragment severely upon protonation,[57] and the nitric acid ester, $(CH_3)_2(NH_2)CCH_2ONO_2$, should it be formed in the particles, is expected to primarily show up at *m/z* 88.076 (NO_2-ejection) and 72.081 (HNO_3-ejection), whereas the protonated molecule signal at *m/z* 135.076 should be almost 2 orders of magnitude smaller. The signals at *m/z* 88.076 and 72.081 also have contributions from 2-amino-2-methylpropanal and AMP, respectively, and it is consequently not possible to resolve by PTR-MS if 2-amino-2-methylpropyl nitrate, $AMPNO_2$ or both are formed in the particle phase in the present experiments.

Reactions similar to (14)-(15) are also foreseen to occur on the particles for both $(CH_3)(CH_2OH)=NH$ and $(CH_3)_2(CHO)CNH_2$ resulting in respectively $(CH_3)(CH_2OH)=NNO_2$ and $(CH_3)_2(CHO)CNHNO_2$, of which the latter was not detected in the present experiments.

Imines undergo addition reactions with water and amines.[54] The two imines formed in the AMP photo-oxidation, $(CH_3)_2C=NH$ and $(CH_3)(CH_2OH)C=NH$, are expected to react with water on particles and chamber walls to give NH_3 and the corresponding ketones $(CH_3)_2CO$ and $(CH_3)(CH_2OH)CO$, respectively. The use of IPN as OH precursor, resulting in acetone, hinders verification of $(CH_3)_2C=NH$ hydrolysis in the chamber, but the *m/z* 75.043 ($C_3H_7O_2^+$) signal, ascribed to hydroxyacetone, is observed in all experiments. We note that the growth the *m/z* 75.043 signal is slightly delayed relative to those of the gas phase products.

The imine exchange reactions with the two primary amines present during the chamber experiments, $(CH_3)_2(CH_2OH)CNH_2$ (AMP) and the primary product $(CH_3)_2(CHO)CNH_2$, will result in $(CH_3)_2C=NC(CH_3)_2CH_2OH$ (expected PTR-MS signals at *m/z* 130.123 / 112.113), $(CH_3)_2C=NC(CH_3)_2CHO$ (expected PTR-MS signal at *m/z* 128.108), $(CH_3)(CH_2OH)C=N-C(CH_3)_2CH_2OH$ (expected PTR-MS signals at *m/z* 146.118 / 128.108) and $(CH_3)(CH_2OH)C=N-C(CH_3)_2CHO$ (expected PTR-MS signals at *m/z* 144.102 / 126.092). None of these imines were detected in the gas phase with ion signal intensity larger than 2% of the decrease in the AMP signal during the experiments.

Table 1. Relevant mass peaks detected by PTR-ToF-MS during AMP photo-oxidation experiments.

m/z	Ion sum formula	Interpretation [a]		Comments
		Neutral molecule	Origin	
18.034	NH_4^+	NH_3	H,F	From imine hydrolysis, fragment from $[AMP]H^+$
31.018	CH_3O^+	CH_2O	P,S	Product in multiple reactions
42.034	$C_2H_4N^+$	CH_3CN	S	From $(CH_3)_2C=NH$. Detected in 3 of 6 experiments.
44.014	CH_2NO^+	HNCO	S,H	From $CHONH_2$. only observed in a few experiments at high E/N
46.029	CH_4NO^+	$CHONH_2$	H	Condensation product from AMP + HCOOH
58.065	$C_3H_8N^+$	$(CH_3)_2C=NH$	P,S	From NH_2-abstraction, secondary product from $(CH_3)_2(NH_2)CCHO$
59.049	$C_3H_7O^+$	$(CH_3)_2CO$	H,F	$(CH_3)_2CHONO$ (IPN), $(CH_3)_2CO$ from IPN, from hydrolysis of $(CH_3)_2C=NH$, secondary product from AMPNO?
60.044	$C_2H_6NO^+$	$CH_3C(O)NH_2$	P,S	From $-CH_3$ abstraction, secondary product from $(CH_3)_2(NH_2)CCHO$ + OH reaction
71.049	$C_4H_7O^+$		H	NH_2NO_2 ejection from $[(CH_3)_2(CHO)CNHNO_2]H^+$, NH_3 ejection from $[(CH_3)_2(NH_2)CCHO]H^+$
72.044	$C_3H_6NO^+$	$CHO(CH_3)C=NH$	S	From $(CH_3)_2(NH_2)CCHO$ + OH
72.081	$C_4H_{10}N^+$		F	H_2O ejection from $[AMP]H^+$
73.065	$C_4H_9O^+$	$CH_2(O)C(CH_3)_2$	H,F	NH_3 ejection from $[AMP]H^+$, NH_2NO_2 ejection from $[AMPNO2]H^+$, H_2O ejection from $[CH_3C(OH)(CH_3)CH_2OH]H^+$, fragment from $[AMPNO]H^+$
74.060	$C_3H_8NO^+$	$HOCH_2(CH_3)C=NH$	P	From $-CH_3$ abstraction
75.043	$C_3H_7O_2^+$	$CH_3C(O)CH_2OH$	H	From hydrolysis of $HOCH_2(CH_3)C=NH$
88.076	$C_4H_{10}NO^+$	$CH_3C(NH_2)(CH_3)CHO$	P	From $-CH_2-$ abstraction
90.092	$C_4H_{12}NO^+$	$CH_3C(NH_2)(CH_3)CH_2OH$		AMP
100.075	$C_5H_{10}NO^+$	$(CH_3)_2(CHO)C-N=CH_2$	H	Condensation product between $(CH_3)_2(NH_2)CCHO$ and CH_2O
102.089	$C_5H_{12}NO^+$	$(CH_3)_2(CH_2OH)C-N=CH_2$	H	Condensation product between AMP and CH_2O
103.049	$C_3H_7N_2O_2^+$	$(CH_3)_2C=NNO_2$	H,S	From $(CH_3)_2C=NH$
116.070	$C_5H_{10}NO_2^+$	$(CH_3)_2(NH_2)CCH_2OC(O)H$	H	Formic acid ester
135.076	$C_4H_{11}N_2O_3^+$	$(CH_3)_2(CH_2OH)CNHNO_2$	P	AMPNO2

[a] Abbreviations: P, primary product; S, secondary product; H, product from heterogeneous chemistry (see text); F, fragment ion.

3.2.3 Particle-phase

Strong particle formation was observed in all the present AMP photo-oxidation experiments alike in the previously reported trials carried out in the UCR EPA [11] and CSIRO [17] indoor environmental chambers. We reiterate that the present experiments are characterized by a low relative humidity of < 2%, which slows the particle growth. Figure 3 illustrates the time evolution of particles, measured by SMPS, displaying number concentrations reaching 10^5 cm^{-3} and a continuous size growth throughout the experiments.

A non-negligent number of particles were already formed during the reactant mixing in the chamber before opening the canopy to solar radiation; these particles were formed in the acid-base reaction of AMP with traces of HNO_3 initially resulting in surface reactions of the added NOx, and later resulting from NO_2 reaction with OH radicals. The AMS shows the AMP nitric acid salt to account for >80% of the total particle mass, and that ammonium nitrate only makes up 3-5% of the mass, see Table S13. The particle yields in the individual experiments are presented in Figure S25.

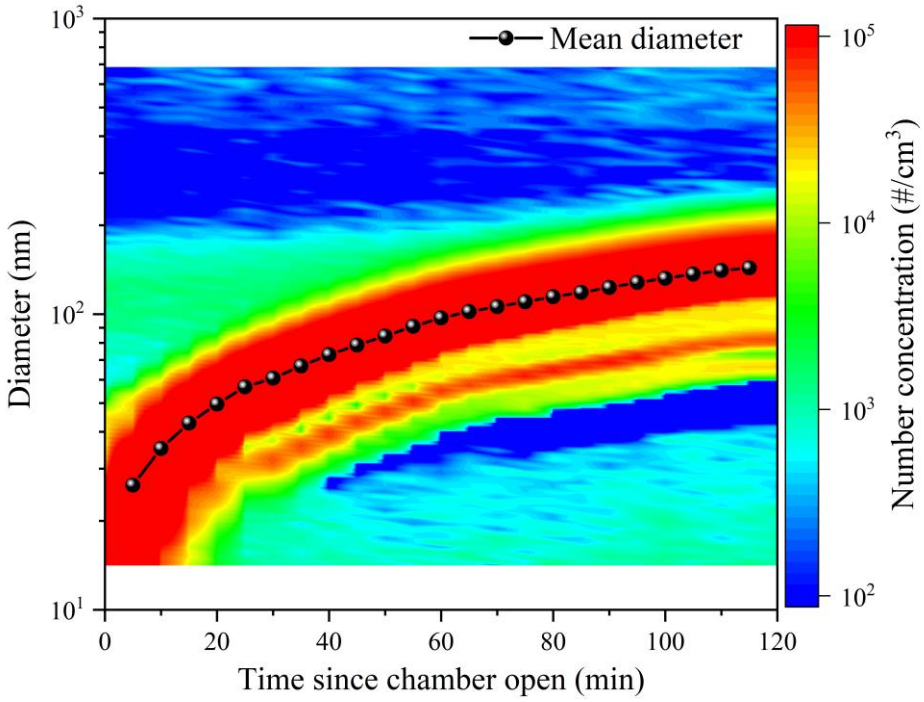

Figure 3 Particle number concentration and particle size distribution as a function of time during the photo-oxidation experiment on 2015.06.15.

Figure 4 shows the time profiles of the relative ion signals obtained by CHARON PTR-ToF-MS. The MS-spectrum is very simple considering that the cutoff in ion signal is 0.5% of the *m/z* 90.092 AMP signal. The AMP nitrate salt (recognizable by *m/z* 90.092, 73.065, 72.081 and 18.034, and 45.993 (NO_2^+)) is the by far dominant particle component. It is also evident from the relative ion intensities that the particles contain very little of the major AMP photo-oxidation products 2-amino-2-methylpropanal (*m/z* 88.076) and propan-2-imine (*m/z* 58.065). The latter is both a primary and secondary photo-oxidation product, but it is a stronger base than both AMP and 2-amino-2-methylpropanal, and may therefore displace these compounds in the particle phase. Also the minor gas phase product from -CH_3 abstraction, $(CH_3)(CH_2OH)C{=}NH$, is identified in the aerosol at *m/z* 74.066. The *m/z* 144.067 and 159.146 peaks are the strongest of a plethora high mass ion signals evidencing particle processing. Only very small amounts of $AMPNO_2$ (*m/z* 135.076) were detected in the particles by CHARON-PTR-MS; Figure 4 includes a 10-fold amplified *m/z* 135.075 signal. Calibration experiments with nano particles containing AMP-nitrate and $AMPNO_2$ place an upper limit of 110 ng/m^3 $AMPNO_2$ in the particles formed during the illustrated photo-oxidation experiment.

A closer inspection of the ion signal time profiles inserted in Figure 4 shows that the profiles of *m/z* 58.065, 74.066, 135.075 and 159.146 all show features indicating aerosol processing. The growths of the *m/z* 58.065 and 74.066 signals from the two imine photo-oxidation products, $(CH_3)_2C{=}NH$ and $(CH_3)(CH_2OH)C{=}NH$, initially resemble that of AMP (*m/z* 90.090), but then change their slope. We interpret this as a sign of commencing gas phase water transfer to the

particle phase resulting in hydrolysis of the two imines to give acetone, hydroxyacetone and NH_3 that are then released to the gas phase, see above.

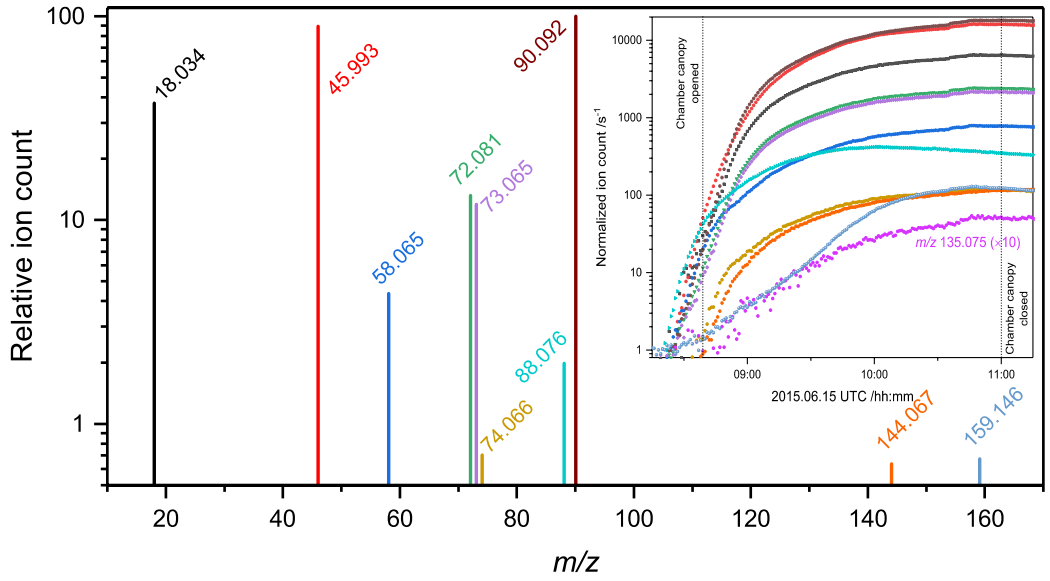

Figure 4. CHARON-PTR-ToF-MS mass spectrum and its time evolution. Ion signals with intensity less than 0.5% of the AMP signal m/z 90.090 at 11:00 UTC, and ion signals related to the ion source and to isotopes are excluded. Data from the AMP photo-oxidation experiment on 2015.06.15.

The $–NHNO_2$ group is acidic and HNO_3 will therefore not drive $AMPNO_2$ partitioning to the particle phase. On the contrary, the temporal profiles of the *m/z* 135.075 gas phase and particle phase signals suggest that $AMPNO_2$ is in part formed in the particle phase and then released to the gas phase. Figure 5 compares the temporal profiles of AMP and the photo-oxidation products $(CH_3)_2(CHO)CNH_2$, $(CH_3)_2C=NH$, $(CH_3)(CH_2OH)C=NH$ and $AMPNO_2$ in the gas and particle phases. It can be seen that $AMPNO_2$ initially increases in the gas phase very much like the other primary photo-oxidation products, but in contrast to the other compounds that level off as AMP decreases, the $AMPNO_2$ ion signal continues to increase – even after the chamber canopy is closed

blocking further photo-oxidation. The same trend is observed in the other experiments (Figures SX-SY) and can only be rationalized in terms of $AMPNO_2$ being formed on the particles.

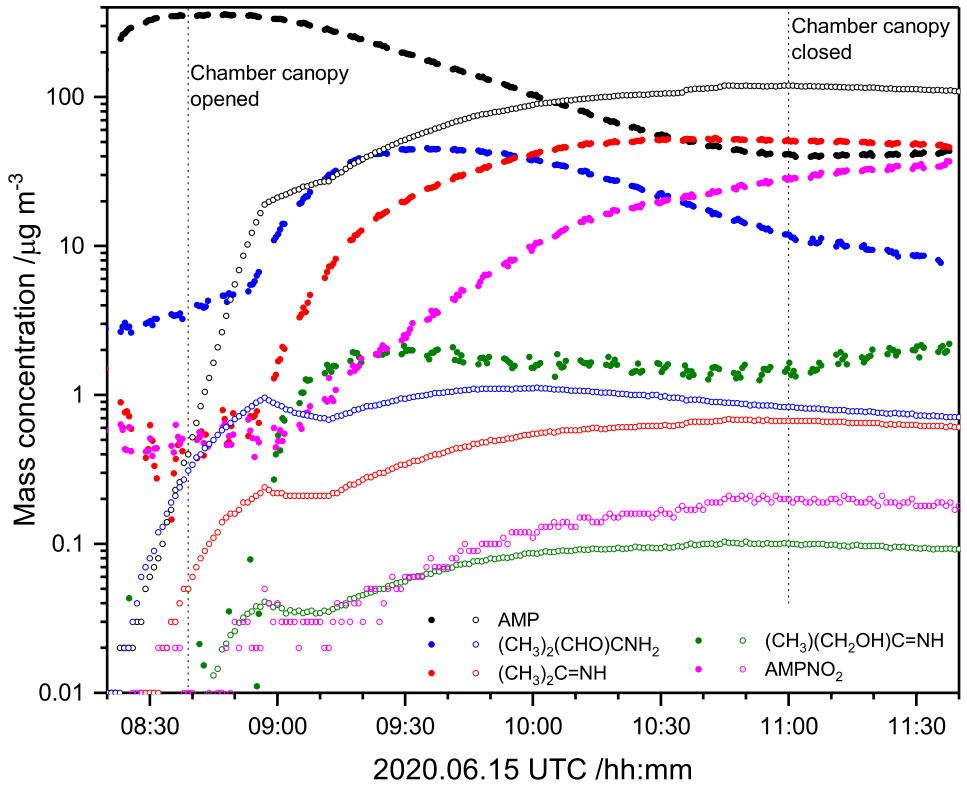

Figure 5. Time evolution of AMP (m/z 90.090), $CH_3C(NH_2)(CH_3)CHO$ (m/z 88.076), $(CH_3)_2C=NH$ (m/z 58.065), $HOCH_2(CH_3)C=NH$ (m/z 74.063) and $AMPNO_2$ (m/z 135.094) in the gas phase (solid) and particle phase (open circles) during the photo-oxidation experiment on 2015.06.15.

Aerosol filter samples were collected at the end of each photo-oxidation experiment. Figure 6 shows the GC×GC-NCD chromatogram for the aerosol filter sample collected at the end of the AMP photo-oxidation experiment on 2015.06.15. The main peak shown is $AMPNO_2$, which was easily detected within the complex matrix due to the combination of two-dimensional GC

separation and nitrogen-specific detection. $AMPNO_2$ was detected in all of the aerosol samples collected at the end of the AMP photo-oxidation experiments; the additional chromatograms can be found Figures S26-S28. Table S14 and S15.

Q: How to rationalize that the filter samples shows tens of microgram per cubic meter of AMP-nitramine (see Table S14) with the CHARON results showing <0.1 microgram per cubic meter.

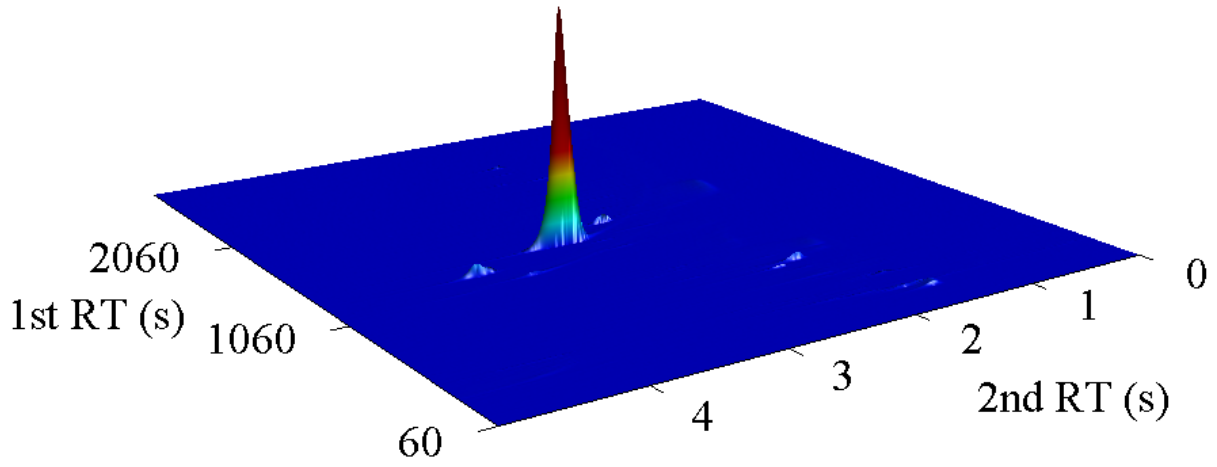

Figure 6. GC×GC-NCD chromatogram to show the detection of $AMPNO_2$ in an aerosol sample collected at the end of the AMP photo-oxidation experiment on 2915.06.15. Several minor organic nitrogen species are also present in the particle phase.

AMP-nitrate volatility was studied using a home-made volatility tandem differential mobility analyzer (VTDMA) [58] employing pure ammonium nitrate as reference. Figure 7 compares the results from volatility measurements of ammonium nitrate and AMP-nitrate. The apparent change in the VFR-curvature for the AMP-nitrate particles between 330 and 345 K may likely be related to the transition from deliquescent to dry particles. The vapor pressure of AMP-nitrate, p^0 = (1.3 ± 0.3) × 10^{-5} Pa at 298 K, and the enthalpy of vaporization, $\Delta_{vap}H$ = 80 ± 16 kJ mol^{-1}, were derived

assuming the evaporation taking place from a liquid and not from a crystalline phase, see Salo et al. for a details.[59]

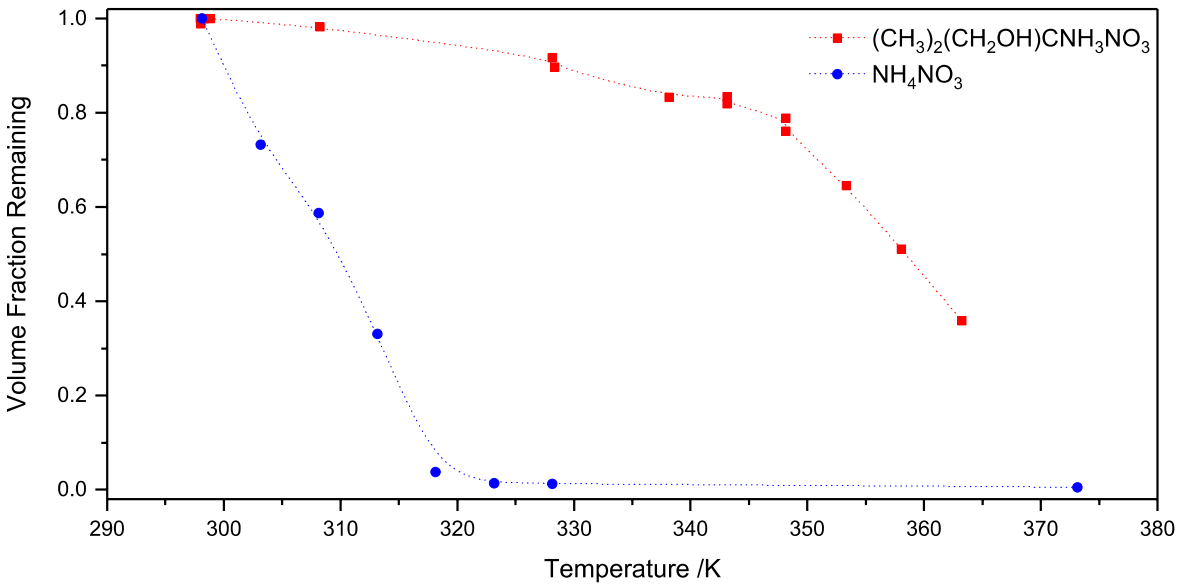

Figure 7. The volume fraction remaining of AMP nitrate (red) and ammonium nitrate (blue) in nanoparticles as measured by VTDMA.

3.3 Gas phase photo-oxidation modelling

The theoretical calculations can only place conservative limits to branching in the AMP + OH reaction; the product distribution within each of the abstraction routes, Scheme 1, is also burdened with uncertainty, although not to the same degree as the branching. Two additional issues arising in connection with the prominent particle formation in the photo-oxidation experiments are: (1) AMP gas-to-particle transfer must be considered explicitly as a sink in modelling the gas phase chemistry, and (2) $AMPNO_2$ formation on particles and subsequent particle-to-gas transfer should be considered.

Restating, the PTR-MS response was calibrated with respect to CH_2O, AMP and $AMPNO_2$, whereas theoretically derived instrumental response factors, summarized in Table S1, were used for other compounds. The uncertainties in calculated volume mixing ratios are estimated to be ±10% for calibrated compounds and ±20% for other compounds. Figure 8 shows the derived mixing ratio time evolutions of AMP and primary photo-oxidation products observed in the 2015.06.15 experiment and amount of AMP incorporated in the aerosol; results for the other experiments are documented in Figures SX-Y. It can be seen that ~40% of AMP is lost to the aerosol phase during this particular experiment.

The mixing ratios for $(CH_3)_2(NH_2)CCHO$, $(CH_3)_2C=NH$, $(CH_3)(CH_2OH)C=NH$ and $(CH_3)_2(CH_2OH)CNHNO_2$ were modelled employing the rate coefficients summarized in Table 2 and the branching ratios given in Table 3. included in Figure 8 includes the for an initial H-abstraction branching of CH_3:CH_2:NH_2 = 0.08 : 0.82 : 0.10.

Table 2. Text

Reaction	Rate coefficient	Reference
$(CH_3)_2(CH_2OH)CNH_2 + OH$	2.8×10^{-11}	[10]
$(CH_3)_2(CHO)CNH_2 + OH$	9.0×10^{-11}	This work
$(CH_3)_2C=NH + OH$ [a]	1.5×10^{-11}	Estimated, this work
$(CH_3)(CH_2OH)C=NH$	2.8×10^{-11}	Estimated, this work
$(CH_3)_2(CH_2OH)CNHNO_2 + OH$ [b]	2.8×10^{-11}	Estimated, this work

[a] 100% NH abstraction. [b] 100% CH_2 abstraction.

Table 3. Branching ratio of the H-abstraction from the -CH_3, -CH_2- and -NH_2 groups in the $(CH_3)_2(CH_2OH)CNH_2$ + OH reaction

Reaction	Experiment					
	1	2	3	4	5	6
$(CH_3)_2(CH_2OH)CNH_2$ + OH	8:80:12	8:80:12	8:80:12	8:80:12	8:80:12	8:80:12

The theoretical calculations place an upper limit of 10% to H-abstraction from the –CH_3 group in the initial AMP + OH reaction. Assuming that $HOCH_2(CH_3)C=NH$ accounts for 60% of products following H-abstraction from the –CH_3 group (see Scheme 1), and that the rate coefficient for reaction with OH radicals is 2.8 × 10^{-11} cm^3 $molecule^{-1}$ s^{-1} (the same as AMP) $CH_3(CH_2OH)C=NH$ subsequently undergoes reaction, places the experimental branching to 8%.

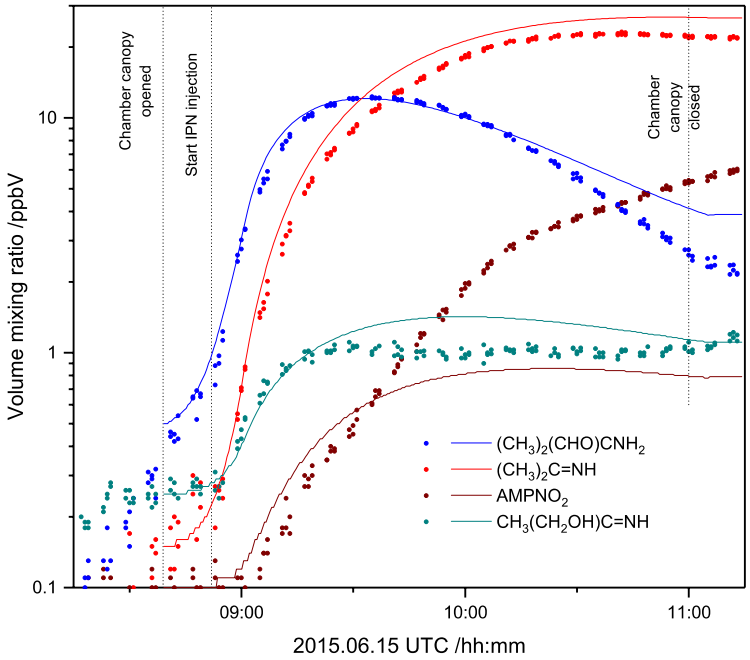

Figure 8. Observed and modelled temporal profiles of products in the OH-initiated AMP photo-oxidation on 2015.06.15.

The *m/z* 73.065 temporal profile differs from all the other ion signals shown in Figure 4 (and Figures SX-SY). The ion signal has established contributions from AMP and AMPNO2, and a potential contribution from AMPNO. No other primary or secondary product in the AMP photo-oxidation that could possibly contribute to the *m/z* 73.065 ion signal was uncovered. After subtracting the known contributions from AMP (2.6% of the *m/z* 90.092 intensity) and $AMPNO_2$ (1.63 times the *m/z* 135.076 intensity), the profile resembles that of a photo-stable secondary product and not that of a chamber artefact. It can therefore unambiguously be concluded that *m/z* 73.065 does not arise from protonated AMPNO (eq. 3a), in which case the signal should have shown a transient profile. The ion sum formula, $C_4H_9O^+$, may correspond to a neutral molecule with formula C_4H_8O of which there are 48 structures listed in ChemSpider.[60] Two of these have a methylpropane backbone, $CH_2=C(CH_3)CH_2OH$ and $(CH_3)_2C=CHOH$, but these compounds cannot be linked to AMP gas phase degradation. The *m/z* 73.065 ion may alternatively be a fragment ion resulting from H_2O ejection, in which case the neutral molecule would have the sum formula $C_4H_{10}O_2$. There are 41 structures with this formula listed in ChemSpider, of which 3 have a methylpropane backbone, but only one that can possibly be linked to AMP gas phase degradation, the diol $CH_3C(OH)(CH_3)CH_2OH$.

The molar balance at 10:30 is 80%

$AMPNO_2$ can be formed either directly in the reaction between AMP and HNO_3 on particle surfaces, or indirectly via the nitrate-ester of AMP, which subsequently acts as a nitro-donor. We do not see a the protonated nitrate ester, ref.[57] so m/z 135 is unique to AMPNO2.

4 CONCLUSIONS

To the best of our knowledge, there are no natural emissions of AMP to the atmosphere. Minor emissions may arise from the use of consumer products containing AMP,[1] but implementation of large-scale CO_2 capture facilities employing AMP-containing solvents may likely result in emissions of a different measure. Once in the atmospheric compartment, AMP will partition between the gas phase and the aerosol phase and undergo photo-oxidation; AMP may also form new particles in homogeneous nucleation with various acidic atmospheric constituents. The competition between the gas phase removal processes mentioned will strongly depend on the local conditions.

With $k_{OH+AMP} \approx 2.8 \times 10^{-11}$ cm^3 molecule^{-1} s^{-1}, the lifetime of AMP with respect to gas phase reaction with OH during daytime will typically be around 10 h. The night-time chemistry of AMP is expected to be dominated by the NO_3 radical. There is no experimental value for k_{NO_3+AMP}, but the empirical correlation between OH and NO_3 rate coefficients for reaction with amines implies a moderate rate coefficient, $k_{NO_3+AMP} \approx 3.7 \times 10^{-14}$ cm^3 molecule^{-1} s^{-1} at 298 K.[6] Assuming an average nighttime NO_3 concentration of around 5×10^8 cm^{-3} [49, 61] brings the estimated lifetime of AMP during nighttime to around 15 h. There is currently no information in the literature on the branching between N–H and C–H abstraction in amines by NO_3.

A detailed mechanism for the OH-initiated atmospheric gas phase photo-oxidation of AMP was obtained by combining results from quantum chemistry-based theoretical calculations and photo-oxidation experiments carried out in a large atmospheric simulation chamber. On the one hand, the theoretical calculations are only able to provide conservative limits to the important branching between N-H and C-H abstraction in the AMP + OH reaction. On the other hand, the theoretical calculations give a precise product distribution within each of the four H-abstraction routes.

Modelling the temporal gas phase product distributions and the aerosol compositions in the photo-oxidation experiments narrows the uncertainty in the initial AMP + OH branching to within a few per cent: ~85% H-abstraction from $–CH_2–$ group, ~8% H-abstraction from $–CH_3$ group, and only ~7% H-abstraction from $–NH_2$ group. The potential of AMP to form carcinogens in the atmosphere is consequently small in comparison to those of MEA[62-64] and PZ.[18]

The major product in the atmospheric AMP photo-oxidation, $CH_3C(NH_2)(CH_3)CHO$, is found to react 4-5 times faster than AMP with OH radicals resulting primarily in $(CH_3)_2C=NH$. This imine is predictably reacting slower than AMP with OH radicals and is therefore projected to hydrolyze to acetone and ammonia under atmospheric conditions. Regarding the photo-oxidation products of health concern, AMPNO and $AMPNO_2$, the former will never build up in the atmosphere due to very fast photolysis and very fast reaction with OH. Should AMPNO transfer to the atmospheric aqueous phase, it will hydrolyze to $CH_3C(OH)(CH_3)CH_2OH$. $AMPNO_2$ is expected to react nearly equally fast with OH as AMP, i.e. the atmospheric lifetime with respect to gas phase photo-oxidation is estimated to be > 10 h. There are no data for the Henry's law solubility constants for nitramines, but to a first approximation they are expected to be the same as those of the nitrosamines, which is 3-10 times larger than the corresponding amine.[65] Consequently, a large fraction of $AMPNO_2$ is expected to transfer to the atmospheric aqueous phase and undergo at least some processing there before surface deposition.

The strong particle growth observed during AMP photo-oxidation experiments suggests that new particle formation may constitute an important gas phase removal process for AMP under atmospheric conditions. The VTDMA studies support this revealing a low vapor pressure of the AMP nitric acid salt, $p^0 = (1.3 \pm 0.3) \times 10^{-5}$ Pa at 298 K. There is only one other alkanolamine-nitrate, for which similar experimental data are available; the vapor pressure of the ethanolamine

(MEA) nitric acid salt is reported to be around 5 times higher, $p^0 = (9.0 \pm 0.4) \times 10^{-5}$ Pa at 298 K,[66] which in part can be rationalized by the difference in basicity ($pK_{b,MEA} = 4.56$; $pK_{b,AMP} = 4.32$).[67] Inferring from the experimental vapor pressures of MEA nitrate [66] and other MEA salts including the sulphate,[68] it is obvious that AMP has a large potential to form new particles.

Assuming that uptake coefficients for methylamines on 59-82 wt % sulfuric acid ($\gamma \sim 2 \times 10^{-2}$) [69] establish the level to be expected for amine uptake on deliquescent particles in general, the aqueous particle uptake of AMP will be diffusion controlled under atmospheric conditions. The Henry volatility of AMP was reported to be $K_H^{px} = 258$ Pa at 40 C (Henry's law solubility H^{cp} = 215 mol m^{-3} Pa^{-1}).[70] Under non-reactive equilibrium conditions and assuming the liquid water content in clouds, fog, and urban aerosol to be respectively 3, 0.2 and 10^{-4} cm^3 m^{-3}, [71] AMP will partition roughly 60, 10 and <<1% to the aqueous particle phase in the three cases. However, urban clouds, fog and deliquescent particles are in general acidic, and the AMP partitioning will therefore be shifted additionally towards the aqueous phase.

There are no experimental rate coefficients for AMP reactions in the aqueous phase; the group contribution method by Minakata et al.[72] predicts $k_{OH,aq} = 5.6 \times 10^9$ M^{-1} s^{-1}. Assuming $[OH]_{av} = 3.5 \times 10^{-15}$ in urban clouds and 4.4×10^{-13} in urban deliquescent particles,[6] the estimated lifetime of AMP in clouds is around 14 h, but only 7 min in deliquescent urban particles. The high reactivity in the deliquescent particle phase will consequently drive additional uptake to the aerosol and a significant amount of AMP will actually be oxidized in deliquescent particles. There are no experimental results from mechanistic studies of aqueous phase AMP reactions, and only speculations on the possible aqueous phase degradation of AMP have been offered.[73] It should be noted that the urban clouds, fog and deliquescent particles in general are acidic, and that AMP therefore will be on its protonated form in aqueous phase. This reduces H-abstraction at the

protonated amino group significantly,[74-76] diminishing the possible formation of AMPNO and $AMPNO_2$. The former will in any case hydrolyze directly to 2-methylpropane-1,2-diol.

The present results permit implementation of a validated AMP gas phase degradation mechanism for emission dispersion modelling. Given that both new particle formation and phase transfer to aqueous and deliquescent particles will be important loss processes for AMP, a computational costly 3D chemistry transport multiphase model will be required to describe the atmospheric fate of AMP appropriately. Realizing that the atmospheric aqueous phase constitutes either a time-delay of AMP degradation or an irreversible sink allows a worst-case scenario calculation based on pure gas phase chemistry.

A simple box-model, based on the atmospheric conditions in the Oslo region, illustrates that the potential health impact of AMP emission from a point source is much lower than those of MEA and PZ (model parameters in Tables S13-S14). The results, shown in Figure 9.

Figure 9. Results from box-modelling the formation of nitrosamines and nitramines in the atmosphere under average conditions in the Oslo region.

ASSOCIATED CONTENT

Supporting Information. Details on instrumentation and methodologies including chemical synthesis. Details on the atmospheric chemistry of piperazine and 1-nitropiperazine from first principles. Details on the piperazine + OH kinetics study. Details on the 1-nitropiperazine photo-oxidation study. Details on the 1-nitrosopiperazine photolysis study. Details on the piperazine

photo-oxidation study. Details on the particle analysis. The Supported Information is available free of charge on the ACS Publications website at DOI: 10.1021/acs/jpca.xxxxxxxx.

AUTHOR INFORMATION

Present Addresses

† School of Environmental and Municipal Engineering, Qingdao University of Technology, Fushun Road 11, Qingdao, 266033 China

*E-mail: c.j.nielsen@kjemi.uio.no Phone: +47-22855680.
ORCID
Armin Wisthaler: 0000-0001-5050-3018
Tomas Mikoviny: 0000-0002-8461-0783
Barbara D'Anna: 0000-0001-8915-4097
Claus Jørgen Nielsen: 0000-0002-2962-2634
Yngve Stenstrøm: 0000-0001-9598-5225
Simen Antonsen: 0000-0002-9416-5476
Jacquiline Fiona Hamilton 0000-0003-0975-4311
Naomi J. Farren: 0000-0002-5668-1648
Wen Tan: 0000-0003-01010313X
Mattias Hallquist: 0000-0001-5691-1231
Yizhen Tang: 0000-0002-5886-5299

Author Contributions

The manuscript was written through contributions of all authors. All authors have given approval to the final version of the manuscript. [§]These authors contributed equally.

ACKNOWLEDGMENT

This work is part of the Atmospheric Chemistry of Amines project (ACA) supported by the CLIMIT program under contract 244055 and has received additional support from the Research Council of Norway through its Centres of Excellence scheme, project number 262695, and from the VISTA-programme, project 6157.

Notes

The authors declare no competing financial interest

REFERENCES

(1) ECHA - European Chemicals Agency. https://echa.europa.eu (accessed December 12, 2020).

(2) Uma Maheswari, A.; Palanivelu, K. Carbon dioxide capture and utilization by alkanolamines in deep eutectic solvent medium. *Ind. Eng. Chem. Res.* **2015,** *54*, 11383-11392.

(3) Sartori, G.; Ho, W.; Savage, D.; Chludzinski, G.; Wlechert, S. Sterically-hindered amines for acid-gas absorption. *Sep. Purif. Methods* **1987,** *16*, 171-200.

(4) Tontiwachwuthikul, P.; Meisen, A.; Lim, C. J. Solubility of carbon dioxide in 2-amino-2-methyl-1-propanol solutions. *J. Chem. Eng. Data* **1991,** *36*, 130-133.

(5) Cousins, A.; Feron, P.; Hayward, J.; Jiang, K.; Zhai, R. *Further assessment of emerging CO2 capture technologies for the power sector and their potential to reduce cost*; CSIRO report EP189975; CSIRO, Australia, 2019.

(6) Nielsen, C. J.; Herrmann, H.; Weller, C. Atmospheric chemistry and environmental impact of the use of amines in carbon capture and storage (CCS). *Chem. Soc. Rev.* **2012,** *41*, 6684-6704.

(7) Låg, M. Health effects of amines and derivatives associated with CO2 capture. 2011. *The Norwegian Institute of Public Health* **2011**, 45.

(8) Murphy, S.; Sorooshian, A.; Kroll, J.; Ng, N.; Chhabra, P.; Tong, C.; Surratt, J.; Knipping, E.; Flagan, R.; Seinfeld, J. Secondary aerosol formation from atmospheric reactions of aliphatic amines. *Atmos. Chem. Phys.* **2007,** *7*, 2313-2337.

(9) Almeida, J.; Schobesberger, S.; Kürten, A.; Ortega, I. K.; Kupiainen-Määttä, O.; Praplan, A. P.; Adamov, A.; Amorim, A.; Bianchi, F.; Breitenlechner, M. Molecular understanding of sulphuric acid–amine particle nucleation in the atmosphere. *Nature* **2013,** *502*, 359.

(10) Harris, G. W.; Pitts, J. N. Rates of reaction of hydroxyl radicals with 2-(dimethylamino)ethanol and 2-amino-2-methyl-1-propanol in the gas phase at 300 ± 2 K. *Environ. Sci. Technol.* **1983,** *17*, 50-51.

(11) Carter, W. P. L. *Reactivity estimates for selected consumer product compounds*; Final Report to the California Air Resources Board Contract No. 06-408; https://intra.cert.ucr.edu/~carter/pubs/aminrep.pdf; 2008.

(12) Carter, W. P. L. *Development of the SAPRC-07 Chemical Mechanism and Updated Ozone Reactivity Scales*; Final report to the California Air Resources Board Contract No. 03-318. August; www.cert.ucr.edu/~carter/SAPRC.; 2007.

(13) Carter, W. P. L. Development of the SAPRC-07 chemical mechanism. *Atmos. Environ.* **2010,** *44*, 5324-5335.

(14) Bråten, H.; Bunkan, A.; Bache-Andreassen, L.; Solimannejad, M.; Nielsen, C. Final report on a theoretical study on the atmospheric degradation of selected amines. *Oslo/kjeller (NILU OR 77/2008)* **2008**.

(15) CCS Norway. https://ccsnorway.com/hse-studies/ (accessed December 12, 2020).

(16) Antonsen, S.; Bunkan, A. J. C.; D'Anna, B.; Eichler, P.; Farren, N.; Hallquist, M.; Hamilton, J. F.; Kvarnliden, H.; Mikoviny, T.; Müller, M., et al. Atmospheric Chemistry of tert-butylamine and AMP. *Energy Procedia* **2017,** *114*, 1026-1032.

(17) Li, K.; White, S.; Zhao, B.; Geng, C.; Halliburton, B.; Wang, Z.; Zhao, Y.; Yu, H.; Yang, W.; Bai, Z., et al. Evaluation of a New Chemical Mechanism for 2-Amino-2-methyl-1-propanol in a Reactive Environment from CSIRO Smog Chamber Experiments. *Environ. Sci. Technol.* **2020,** *54*, 9844-9853.

(18) Tan, W.; Zhu, L.; Mikoviny, T.; Nielsen, C. J.; Wisthaler, A.; D´Anna, B.; Antonsen, S.; Stenstrøm, Y.; Farren, N. J.; Hamilton, J. F., et al. Experimental and Theoretical Study on the OH-Initiated Degradation of Piperazine under Simulated Atmospheric Conditions. *J. Phys. Chem. A* **2020,** *Submitted jp-2020-102238*.

(19) Tan, W.; Zhu, L.; Mikoviny, T. s.; Nielsen, C. J.; Wisthaler, A.; Eichler, P.; Müller, M.; D'Anna, B.; Farren, N. J.; Hamilton, J. F. Theoretical and Experimental Study on the Reaction of tert-Butylamine with OH Radicals in the Atmosphere. *J. Chem. Phys. A* **2018,** *122*, 4470-4480.

(20) Becker, K. H., *The European Photoreactor EUPHORE: Design and Technical Development of the European Photoreactor and First Experimental Results: Final Report of the EC-Project: Contract EV5V-CT92-0059: Funding Period, January 1993-December 1995*. 1996.

(21) Eichler, P.; Muller, M.; D'Anna, B.; Wisthaler, A. A novel inlet system for online chemical analysis of semi-volatile submicron particulate matter. *Atmospheric Measurement Techniques* **2015,** *8*, 1353-1360.

(22) Eichler, P.; Müller, M.; Rohmann, C.; Stengel, B.; Orasche, J. r.; Zimmermann, R.; Wisthaler, A. Lubricating oil as a major constituent of ship exhaust particles. *Environ. Sci. Technol. Lett.* **2017,** *4*, 54-58.

(23) Drewnick, F.; Hings, S. S.; DeCarlo, P.; Jayne, J. T.; Gonin, M.; Fuhrer, K.; Weimer, S.; Jimenez, J. L.; Demerjian, K. L.; Borrmann, S., et al. A New Time-of-Flight Aerosol Mass Spectrometer (TOF-AMS)—Instrument Description and First Field Deployment. *Aerosol Sci. Technol.* **2005,** *39*, 637-658.

(24) Antonsen, S.; Aursnes, M.; Gallantree-Smith, H.; Dye, C.; Stenstroem, Y. Safe synthesis of alkylhydroxy and alkylamino nitramines. *Molecules* **2016,** *21*, 1738/1-1738/8.

(25) Zhao, Y.; Truhlar, D. G. The M06 suite of density functionals for main group thermochemistry, thermochemical kinetics, noncovalent interactions, excited states, and transition elements: two new functionals and systematic testing of four M06-class functionals and 12 other functionals. *Theor. Chem. Acc.* **2008,** *120*, 215-241.

(26) Dunning Jr, T. H. Gaussian basis sets for use in correlated molecular calculations. I. The atoms boron through neon and hydrogen. *J. Chem. Phys.* **1989,** *90*, 1007-1023.

(27) Kendall, R. A.; Dunning Jr, T. H.; Harrison, R. J. Electron affinities of the first-row atoms revisited. Systematic basis sets and wave functions. *J. Chem. Phys.* **1992,** *96*, 6796-6806.

(28) Knizia, G.; Adler, T. B.; Werner, H.-J. Simplified CCSD (T)-F12 methods: Theory and benchmarks. *J. Chem. Phys.* **2009,** *130*, 054104.

(29) Curtiss, L. A.; Redfern, P. C.; Raghavachari, K. Gaussian-4 theory. *J. Chem. Phys.* **2007,** *126*, 084108.

(30) Su, T. Parametrization of kinetic energy dependences of ion–polar molecule collision rate constants by trajectory calculations. *J. Chem. Phys.* **1994,** *100*, 4703-4703.

(31) Vosko, S. H.; Wilk, L.; Nusair, M. Accurate spin-dependent electron liquid correlation energies for local spin-density calculations - a critical analysis. *Can. J. Phys.* **1980,** *58*, 1200-1211.

(32) Lee, C.; Yang, W.; Parr, R. G. Development of the Colle-Salvetti correlation-energy formula into a functional of the energy density. *Phys. Rev. B* **1988,** *37*, 785-789.

(33) Becke, A. D. Density-functional thermochemistry. III. The role of exact exchange. *J. Chem. Phys.* **1993,** *98*, 5648-5652.

(34) Stephens, P. J.; Devlin, F. J.; Chabalowski, C. F.; Frisch, M. J. Ab Initio Calculation of Vibrational Absorption and Circular Dichroism Spectra Using Density Functional Force Fields. *J. Phys. Chem.* **1994,** *98*, 11623-7.

(35) Frisch, M. J.; Trucks, G.; Schlegel, H. B.; Scuseria, G. E.; Robb, M. A.; Cheeseman, J. R.; Scalmani, G.; Barone, V.; Mennucci, B.; Petersson, G. *Gaussian 09, revision B. 01*, Wallingford, CT, 2009.

(36) Frisch, M. J.; Trucks, G. W.; Schlegel, H. B.; Scuseria, G. E.; Robb, M. A.; Cheeseman, J. R.; Scalmani, G.; Barone, V.; Petersson, G. A.; Nakatsuji, H., et al. *Gaussian 16 Rev. C.01*, Wallingford, CT, 2016.

(37) Werner, H. J.; Knowles, P. J.; Knizia, G.; Manby, F. R.; Schütz, M. Molpro: a general-purpose quantum chemistry program package. *Wiley Interdiscip. Rev.: Comput. Mol. Sci.* **2012,** *2*, 242-253.

(38) Glowacki, D. R.; Liang, C.-H.; Morley, C.; Pilling, M. J.; Robertson, S. H. MESMER: An Open-Source Master Equation Solver for Multi-Energy Well Reactions. *J. Chem. Phys. A* **2012,** *116*, 9545-9560.

(39) Coxon, J. A.; Foster, S. C. Radical dependenca of spin-orbit and L-doubling parameters in the X^2P ground-state of hydroxyl. *J. Mol. Spectrosc.* **1982,** *91*, 243-254.

(40) Georgievskii, Y.; Klippenstein, S. J. Long-range transition state theory. *J. Chem. Phys.* **2005,** *122*, 194103.

(41) Miller, W. H. Tunneling corrections to unimolecular rate constants, with application to formaldehyde. *J. Am. Chem. Soc.* **1979,** *101*, 6810-6814.

(42) Tully, F. P. Catalytic dehydration of alcohols by OH. $(H_3C)_3CCH_2OH$: A limiting case. *Symp. (Int.) Combust.* **1991,** *23*, 147-153.

(43) D'Anna, B.; Andresen, Ø.; Gefen, Z.; Nielsen, C. J. Kinetic study of OH and NO3 radical reactions with 14 aliphatic aldehydes. *Phys. Chem. Chem. Phys.* **2001,** *3*, 3057-3063.

(44) Atkinson, R.; Baulch, D. L.; Cox, R. A.; Crowley, J. N.; Hampson, R. F.; Hynes, R. G.; Jenkin, M. E.; Rossi, M. J.; Troe, J. Evaluated kinetic and photochemical data for atmospheric chemistry: Volume II - gas phase reactions of organic species. *Atmos. Chem. Phys.* **2006,** *6*, 3625-4055.

(45) Lindley, C. R. C.; Calvert, J. G.; Shaw, J. H. Rate Studies of the Reactions of the $(CH_3)_2N$ Radical with O_2, NO, and NO_2. *Chemical Physics Letters* **1979,** *67*, 57-62.

(46) Lazarou, Y. G.; Kambanis, K. G.; Papagiannakopoulos, P. Gas-Phase Reactions of $(CH_3)_2N$ Radicals with NO and NO_2. *Journal of Physical Chemistry* **1994,** *98*, 2110-2115.

(47) Tang, Y.; Hanrath, M.; Nielsen, C. J. Do primary nitrosamines form and exist in the gas phase? A computational study of CH_3NHNO and $(CH_3)_2NNO$. *Phys. Chem. Chem. Phys.* **2012,** *14*, 16365-16370.

(48) da Silva, G. Formation of Nitrosamines and Alkyldiazohydroxides in the Gas Phase: The CH_3NH + NO Reaction Revisited. *Environ. Sci. Technol.* **2013,** *47*, 7766-7772.

(49) Wayne, R. P.; Barnes, I.; Biggs, P.; Burrows, J. P.; Canosamas, C. E.; Hjorth, J.; Lebras, G.; Moortgat, G. K.; Perner, D.; Poulet, G., et al. The Nitrate Radical - Physics, Chemistry, and the Atmosphere. *Atmos. Environ., Part A* **1991,** *25*, 1-203.

(50) Borduas, N.; da Silva, G.; Murphy, J. G.; Abbatt, J. P. D. Experimental and Theoretical Understanding of the Gas Phase Oxidation of Atmospheric Amides with OH Radicals: Kinetics, Products, and Mechanisms. *J. Chem. Phys. A* **2015,** *119*, 4298-4308.

(51) Bunkan, A. J. C.; Tang, Y.; Sellevåg, S. R.; Nielsen, C. J. Atmospheric Gas Phase Chemistry of $CH_2{=}NH$ and HNC. A First-Principles Approach. *J. Chem. Phys. A* **2014,** *118*, 5279-5288.

(52) Akbar Ali, M.; Barker, J. R. Comparison of Three Isoelectronic Multiple-Well Reaction Systems: OH + CH_2O, OH + CH_2CH_2, and OH + CH_2NH. *J. Chem. Phys. A* **2015,** *119*, 7578-92.

(53) Challis, B. C.; Challis, J. A., In *The Chemistry of amino, nitroso, and nitro compounds and their derivatives*, Patai, P., Ed. Wiley: Chichester, 1982; pp 1151-1223.

(54) Layer, R. W. Chemistry of Imines. *Chem. Rev.* **1963,** *63*, 489-510.

(55) Mascavage, L. M.; Sonnet, P. E.; Dalton, D. R. On the Surface-Catalyzed Reaction between the Gases 2,2-Dimethylpropanal and Methanamine. Formation of Active-Site Imines. *J. Org. Chem.* **2006,** *71*, 3435-3443.

(56) Zhu, L.; Mikoviny, T.; Wisthaler, A.; Nielsen, C. J. A sampling line artifact in stack emission measurement of alkanolamine-enabled carbon capture facility: surface reaction of amines with formaldehyde. **2017,** *114*, 1022-1025.

(57) Duncianu, M.; David, M.; Kartigueyane, S.; Cirtog, M.; Doussin, J. F.; Picquet-Varrault, B. Measurement of alkyl and multifunctional organic nitrates by proton-transfer-reaction mass spectrometry. *Atmos. Meas. Tech.* **2017,** *10*, 1445-1463.

(58) Jonsson, Å. M.; Hallquist, M.; Saathoff, H. Volatility of secondary organic aerosols from the ozone initiated oxidation of α-pinene and limonene. *J. Aerosol Sci* **2007,** *38*, 843-852.

(59) Salo, K.; Jonsson, Å. M.; Andersson, P. U.; Hallquist, M. Aerosol Volatility and Enthalpy of Sublimation of Carboxylic Acids. *J. Chem. Phys. A* **2010,** *114*, 4586-4594.

(60) ChemSpider. https://www.chemspider.com.

(61) Atkinson, R. Kinetics and Mechanisms of the Gas-Phase Reactions of the NO_3 Radical with Organic Compounds. *J. Phys. Chem. Ref. Data* **1991,** *20*, 459-507.

(62) Nielsen, C. J.; D'Anna, B.; Dye, C.; Graus, M.; Karl, M.; King, S.; Maguto, M. M.; Müller, M.; Schmidbauer, N.; Stenstrøm, Y., et al. Atmospheric chemistry of 2-aminoethanol (MEA). *Energy Procedia* **2011,** *4*, 2245-2252.

(63) Karl, M.; Dye, C.; Schmidbauer, N.; Wisthaler, A.; Mikoviny, T.; D'Anna, B.; Müller, M.; Borrás, E.; Clemente, E.; Muñoz, A. Study of OH-initiated degradation of 2-aminoethanol. *Atmos. Chem. Phys.* **2012,** *12*, 1881-1901.

(64) Onel, L.; Blitz, M. A.; Breen, J.; Rickard, A. R.; Seakins, P. W. Branching ratios for the reactions of OH with ethanol amines used in carbon capture and the potential impact on carcinogen formation in the emission plume from a carbon capture plant. *Physical Chemistry Chemical Physics* **2015,** *17*, 25342-25353.

(65) Sander, R. Compilation of Henry's Law Constants (version 4.0) for Water as Solvent. *Atmos. Chem. Phys.* **2015,** *15*, 4399-4981.

(66) Salo, K.; Westerlund, J.; Andersson, P. U.; Nielsen, C.; D'Anna, B.; Hallquist, M. Thermal Characterization of Aminium Nitrate Nanoparticles. *J. Phys. Chem. A* **2011,** *115*, 11671-11677.

(67) Hamborg, E. S.; Versteeg, G. F. Dissociation Constants and Thermodynamic Properties of Amines and Alkanolamines from (293 to 353) K. *J. Chem. Eng. Data* **2009,** *54*, 1318-1328.

(68) Fan, X.; Dawson, J.; Chen, M.; Qiu, C.; Khalizov, A. Thermal Stability of Particle-Phase Monoethanolamine Salts. *Environ. Sci. Technol.* **2018,** *52*, 2409-2417.

(69) Wang, L.; Lal, V.; Khalizov, A. F.; Zhang, R. Heterogeneous Chemistry of Alkylamines with Sulfuric Acid: Implications for Atmospheric Formation of Alkylaminium Sulfates. *Environ. Sci. Technol.* **2010,** *44*, 2461-2465.

(70) Du, Y.; Yuan, Y.; Rochelle, G. T. Volatility of amines for CO_2 capture. *Int. J. Greenhouse Gas Control* **2017,** *58*, 1-9.

(71) Herrmann, H. Kinetics of Aqueous Phase Reactions Relevant for Atmospheric Chemistry. *Chem. Rev.* **2003,** *103*, 4691-4716.

(72) Minakata, D.; Li, K.; Westerhoff, P.; Crittenden, J. Development of a Group Contribution Method To Predict Aqueous Phase Hydroxyl Radical (HO•) Reaction Rate Constants. *Environ. Sci. Technol.* **2009,** *43*, 6220-6227.

(73) Nielsen, C. J.; Hoffmann, D.; Herrmann, H. *Theoretical evaluation of the fate of harmful compounds post emission*; Report 2210040-3; https://ccsnorway.com/wp-content/uploads/sites/6/2019/10/atmosphericformation_teltek-2.pdf; Tel-Tek: Porsgrunn, 2010.

(74) Simić, M.; Neta, P.; Hayon, E. Pulse radiolytic investigation of aliphatic amines in aqueous solution. *Int. J. Radiat. Phys. Chem.* **1971,** *3*, 309-320.

(75) Getoff, N.; Schwörer, F. Pulsradiolyse von methylamin in wässeriger Lösung. *Int. J. Radiat. Phys. Chem.* **1971,** *3*, 429-439.

(76) Getoff, N.; Schwörer, F. Pulse radiolysis of ethyl, n-propyl, n-butyl and n-amyl amine in aqueous solutions. *Int. J. Radiat. Phys. Chem.* **1973,** *5*, 101-111.